Available online at www.sciencedirect.com
SCIENCE DIRECT®
International Journal of Solids and Structures 42 (2005) 2059–2088
INTERNATIONAL JOURNAL OF SOLIDS and STRUCTURES
www.elsevier.com/locate/ijsolstr

Free-vibration analysis of laminated plates with embedded shear-mode piezoceramic layers

Jean-François Deü [a], Ayech Benjeddou [b,*]

[a] *Conservatoire National des Arts et Métiers, Structural Mechanics and Coupled Systems Laboratory, 2 rue Conté, 75003 Paris, France*
[b] *Institut Supérieur de Mécanique de Paris, LISMMA/Structures, 3 rue Fernand Hainault, 93407 Saint Ouen Cedex, France*

Received 12 January 2004; received in revised form 1 September 2004

Abstract

This paper presents a three-dimensional *exact mixed state space solution* and a parametric analysis for the free-vibration of simply-supported laminates with embedded transverse *shear mode* piezoceramic layers. The formulation retains, as state variables, the standard mechanical displacements and transverse stresses augmented with the electric transverse displacement and potential. It considers both *non-electroded* and *electroded* inner *x-poled* piezoceramic laminae. The solution validation is made through some demonstrated expected results. Then, a parametric study is conducted for various parameters variations. It was found that the thickness distributions of the electric state variables depend strongly on the electric boundary conditions and mode type. Moreover, in contrary to the common practice of the mechanical community, the small difference between short- and open-circuit natural frequencies should not be neglected but can be used to assess the piezoelectric effect through the so-called *effective modal electromechanical coupling coefficient*. Its level was found to depend on the poling direction, mode type, plate length-to-thickness ratio and piezoceramic lamina thickness and position in the laminate. This exact solution and its obtained results can be used for future reference and shear-mode piezoelectric vibration behavior comprehension purposes.

Keywords: Analytical solutions; Free-vibration; Piezoelectric; Adaptive structures; Simply-supported; Mixed state space method; Shear-mode piezoceramic

* Corresponding author. Tel.: +33 1 4945 2979; fax: +33 1 4945 2929.
E-mail address: benjeddou@supmeca.fr (A. Benjeddou).

0020-7683/$ - see front matter © 2004 Elsevier Ltd. All rights reserved.
doi:10.1016/j.ijsolstr.2004.09.003

1. Introduction

Theoretical modeling and simulation of smart structures is an active area of research since the early 1990s. Hence, for the purpose of verifying the accuracy of the wide used approximate theories or computational models of piezoelectric adaptive structures (Saravanos and Heyliger, 1999; Benjeddou, 2000), the interest for exact, closed-form and other analytical solutions has much increased during the last half decade. These low-cost validation techniques are generally developed for static or free-vibration analyses of simply-supported (SS) plate-like structures. Thus, several three-dimensional (3D) exact (Heyliger and Saravanos, 1995; Xu et al., 1997) or approximate (Batra and Liang, 1997; Ding et al., 2000) and two-dimensional (2D) closed-form (Benjeddou and Deü, 2002) solutions have been proposed in the literature for the free-vibration analysis of SS piezoelectric laminated plates. Both through-the-thickness exponential distribution methods (Heyliger and Saravanos, 1995; Batra and Liang, 1997) and state space approaches (Xu et al., 1997; Ding et al., 2000) have been used for the free-vibration problem formulation. The former methods have the advantage of providing explicit expressions, but cumbersome, of the through-the-thickness distributions of the retained electromechanical variables; they also require the solution of an eighth-order ill conditioned *transcendental* equation. In the contrary, state space methods are becoming very popular for exact solutions of various layered adaptive structures problems, such as Saint–Venant end effects in piezoelectric laminates (Tarn and Huang, 2002), axisymmetric problems in layered piezoelectric media (Wang et al., 2002), piezothermoelastic behavior (Tarn, 2002; Zhang et al., 2002), functionally gradient piezoelectric materials (Zhong and Shang, 2003) and magneto-electro-elastic laminates (Wang et al., 2003).

Careful analysis of the above contributions indicates that they have concerned through-the-thickness poled (*extension mode*) piezoelectric materials only. However, although the *shear mode* (in-plane poled) piezoceramics had retained much attention during the last decade, only few papers exist on its application to adaptive plates (Zhang and Sun, 1999; Benjeddou and Deü, 2001a,b; Vel and Batra, 2001a,b). Nevertheless, these had focused on static analyses only. It is then the purpose of this work to present a 3D exact mixed state space solution for the free-vibrations of SS laminates with embedded transverse shear-mode piezoceramic layers. In contrary to the *control theory type* state space approach (Vel and Batra, 2001a), the present *mixed type* one has the great advantage that the size of the system to be solved is independent of the number of layers and is of order four for the laminate with embedded non-electroded piezoceramic laminae and of order three for the laminate with embedded electroded laminae. Also in contrary to the common practice, where the matrix exponential is evaluated analytically (Lee and Jiang, 1996; Chen et al., 1998; Vel and Batra, 2001b), here this task is made numerically.

The available 3D exact or analytical solutions for the free-vibration of simply-supported (SS) piezoelectric laminates have been limited not only to *extension mode* piezoelectric materials but also to the fundamental mode (Xu et al., 1997), few bending modes (Batra and Liang, 1997; Ding et al., 2000) or few thickness modes (Heyliger and Saravanos, 1995). Thus, neither of these solutions was self-contained to be used as a reference solution for other approximate numerical or 2D closed-form solutions (Benjeddou et al., 2002). Liang and Batra (1997) have also presented, in a Technical Note, the unique parametric analysis on changes in frequencies due to embedded *extension mode* piezoelectric layers. All of the previous exact or analytical solutions, except that of Ding et al. (2000), have missed the so-called *special modes* due to nil x-axis ($m_x = 0$) or y-axis ($m_y = 0$) wave numbers. The latter were briefly studied recently by Batra and Aimmanee (2003).

Exact 3D free-vibration analyses of SS piezoelectric composite plates with embedded shear-mode (x-poled) piezoceramic layers have been conducted only recently (Deü and Benjeddou, 2002; Benjeddou and Deü, 2003). The authors have presented detailed parametric studies of the *electromechanical coupling coefficient* (EMCC) of the thickness modes in terms of the plate length-to-thickness ratio for both short-circuited (SC) and open-circuited (OC) frequencies (Deü and Benjeddou, 2002). They have also analyzed the influence of the shear piezoceramic core thickness ratio, the sandwich elastic faces lamination scheme,

and the piezoceramic lamina thickness position for elastic (EL), non-electroded (NE) and SC/OC electroded laminae (Benjeddou and Deü, 2003). However, the latter two references have, unfortunately, missed the special ($m_x = 0$ or $m_y = 0$) modes mentioned in (Ding et al., 2000; Batra and Aimmanee, 2003).

In the following the paper will focuse first on the state space formulation for a generic *x-poled* piezoelectric lamina; then, the exact free-vibration solution is detailed. In particular, the transfer matrices for inner NE and electroded, either SC or OC, piezoelectric laminae are derived. The special case of elastic laminae is also treated. Next, the assembly procedure is described for the different electric boundary conditions (EBC). After discussing the possible implementation and computational aspects of the proposed exact 3D mixed state space approach (MSSA), its validation is presented. For this, some expected theoretical results are first demonstrated for a sandwich SS plate with a shear-mode piezoceramic core and conducting elastic faces. The obtained results are compared to elastic 3D ones from a general purpose commercial finite element (FE) code. The *special modes* (Ding et al., 2000; Batra and Aimmanee, 2003) are briefly presented and analyzed for the first time in this section. A detailed parametric analysis is then conducted to show the influence of the electric boundary conditions (EBC), plate side-to-thickness ratio and piezoceramic lamina thickness and position on the EMCC of both in-plane $(m_x, m_y, 1)$ and thickness $(1, 1, m_z)$ modes. The results are either tabulated or presented in Figures for future *self-contained reference* versus approximate numerical or closed-form 2D solutions.

2. Piezoelectric laminae state space formulation

Consider a rectangular adaptive composite plate of length L_x, width L_y, total thickness H and made of N orthotropic layers (elastic or piezoelectric). The latter can have different thickness and material properties, but with material axes parallel to those of the adopted rectangular co-ordinate system (Fig. 1). The plate is mechanically unloaded while its piezoelectric laminae are polarized along their local x-axis and could be either charge-free, for OC upper and lower surface electrodes, or free of electric potential for SC electrodes.

The 3D linear constitutive equations of the kth piezoelectric lamina, polarized along its material first axis (x_1), is for the converse and direct piezoelectric effects, respectively,

$$\begin{aligned}
\sigma_{xx}^{(k)} &= C_{11}^{(k)}\epsilon_{xx}^{(k)} + C_{12}^{(k)}\epsilon_{yy}^{(k)} + C_{13}^{(k)}\epsilon_{zz}^{(k)} - e_{11}^{(k)}E_x^{(k)} \\
\sigma_{yy}^{(k)} &= C_{12}^{(k)}\epsilon_{xx}^{(k)} + C_{22}^{(k)}\epsilon_{yy}^{(k)} + C_{23}^{(k)}\epsilon_{zz}^{(k)} - e_{12}^{(k)}E_x^{(k)} \\
\sigma_{zz}^{(k)} &= C_{13}^{(k)}\epsilon_{xx}^{(k)} + C_{23}^{(k)}\epsilon_{yy}^{(k)} + C_{33}^{(k)}\epsilon_{zz}^{(k)} - e_{13}^{(k)}E_x^{(k)} \\
\sigma_{yz}^{(k)} &= C_{44}^{(k)}\gamma_{yz}^{(k)} \\
\sigma_{xz}^{(k)} &= C_{55}^{(k)}\gamma_{xz}^{(k)} - e_{35}^{(k)}E_z^{(k)} \\
\sigma_{xy}^{(k)} &= C_{66}^{(k)}\gamma_{xy}^{(k)} - e_{26}^{(k)}E_y^{(k)}
\end{aligned} \tag{1}$$

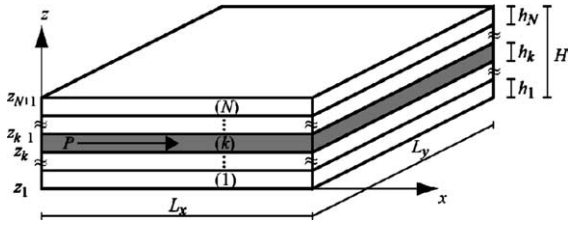

Fig. 1. Adaptive composite plate: polarization, geometry and notations.

$$\begin{aligned} d_x^{(k)} &= e_{11}^{(k)}\epsilon_{xx}^{(k)} + e_{12}^{(k)}\epsilon_{yy}^{(k)} + e_{13}^{(k)}\epsilon_{zz}^{(k)} + \epsilon_{11}^{(k)}E_x^{(k)} \\ d_y^{(k)} &= e_{26}^{(k)}\gamma_{xy}^{(k)} + \epsilon_{22}^{(k)}E_y^{(k)} \\ d_z^{(k)} &= e_{35}^{(k)}\gamma_{xz}^{(k)} + \epsilon_{33}^{(k)}E_z^{(k)} \end{aligned} \tag{2}$$

where σ_{ij} and d_i $(i,j = x,y,z)$ are the stress tensor and the electric displacement vector components; C_{IJ}, e_{kJ} and $\in_{kl}$ $(k, l = 1,2,3; I, J = 1,\ldots,6)$ denote elastic, piezoelectric and dielectric material constants. The strain tensor ϵ_{ij} and electric field vector E_i components are linked to the mechanical displacements u_i and electric potential ϕ by the usual gradient relations. Substituting the latter in Eqs. (1) and (2), then combining some of the resulting equations provide the transverse derivatives of the mechanical displacements and electric potential (a comma states for partial differentiation),

$$\begin{aligned} u_{x,z}^{(k)} &= \frac{\epsilon_{33}^{(k)}}{\Delta_{35}^{(k)}}\sigma_{xz}^{(k)} + \frac{e_{35}^{(k)}}{\Delta_{35}^{(k)}}d_z^{(k)} - u_{z,x}^{(k)} \\ u_{y,z}^{(k)} &= \frac{1}{C_{44}^{(k)}}\sigma_{yz}^{(k)} - u_{z,y}^{(k)} \\ \phi_{,z}^{(k)} &= \frac{e_{35}^{(k)}}{\Delta_{35}^{(k)}}\sigma_{xz}^{(k)} - \frac{C_{55}^{(k)}}{\Delta_{35}^{(k)}}d_z^{(k)} \\ u_{z,z}^{(k)} &= -\frac{C_{13}^{(k)}}{C_{33}^{(k)}}u_{x,x}^{(k)} - \frac{C_{23}^{(k)}}{C_{33}^{(k)}}u_{y,y}^{(k)} - \frac{e_{13}^{(k)}}{C_{33}^{(k)}}\phi_{,x}^{(k)} + \frac{1}{C_{33}^{(k)}}\sigma_{zz}^{(k)} \end{aligned} \tag{3}$$

where

$$\Delta_{35}^{(k)} = C_{55}^{(k)}\epsilon_{33}^{(k)} + e_{35}^{(k)2}$$

The last relation of Eq. (3) is then substituted in the *in plane* stresses and electric displacements of Eqs. (1) and (2), written in terms of the mechanical displacements and electric potential, in order to transform them into the following matrix form,

$$\{y\}^{(k)} = [b]^{(k)}\{x_1\}^{(k)} \tag{4}$$

where

$$\{y\} = \begin{Bmatrix} \sigma_{xx} \\ \sigma_{yy} \\ d_x \\ \sigma_{xy} \\ d_y \end{Bmatrix}, \quad [b] = \begin{bmatrix} C_{11}^{*}\frac{\partial}{\partial x} & C_{12}^{*}\frac{\partial}{\partial y} & e_{11}^{*}\frac{\partial}{\partial x} & \frac{C_{13}}{C_{33}} \\ C_{12}^{*}\frac{\partial}{\partial x} & C_{22}^{*}\frac{\partial}{\partial y} & e_{12}^{*}\frac{\partial}{\partial x} & \frac{C_{23}}{C_{33}} \\ e_{11}^{*}\frac{\partial}{\partial x} & e_{12}^{*}\frac{\partial}{\partial y} & -\epsilon_{11}^{*}\frac{\partial}{\partial x} & \frac{e_{13}}{C_{33}} \\ C_{66}\frac{\partial}{\partial y} & C_{66}\frac{\partial}{\partial x} & e_{26}\frac{\partial}{\partial y} & 0 \\ e_{26}\frac{\partial}{\partial y} & e_{26}\frac{\partial}{\partial x} & -\epsilon_{22}\frac{\partial}{\partial y} & 0 \end{bmatrix}, \quad \{x_1\} = \begin{Bmatrix} u_x \\ u_y \\ \phi \\ \sigma_{zz} \end{Bmatrix}$$

$$C_{\alpha\beta}^{*(k)} = C_{\alpha\beta}^{(k)} - \frac{C_{\alpha 3}^{(k)}C_{\beta 3}^{(k)}}{C_{33}^{(k)}}, \quad e_{1\alpha}^{*(k)} = e_{1\alpha}^{(k)} - \frac{e_{13}^{(k)}C_{\alpha 3}^{(k)}}{C_{33}^{(k)}}, \quad \epsilon_{11}^{*(k)} = \epsilon_{11}^{(k)} + \frac{e_{13}^{(k)2}}{C_{33}^{(k)}}; \quad \alpha,\beta = 1,2$$

The electrodynamics response of the kth piezoelectric lamina, free of mechanical and electric body loads, is governed by the classical stress and charge equations, respectively. After the substitution of the in-plane constitutive equations, Eq. (4), in these equations of motion and the solution for the thickness first derivatives of the transverse stresses and electric displacement, the following relations are obtained (ρ is the mass density and a dot denotes a time differentiation),

$$
\begin{aligned}
\sigma_{zz,z}^{(k)} &= \rho\ddot{u}_z^{(k)} - \sigma_{xz,x}^{(k)} - \sigma_{yz,y}^{(k)} \\
\sigma_{xz,z}^{(k)} &= \rho\ddot{u}_x^{(k)} - \left[\left(C_{11}^{*(k)}\frac{\partial^2}{\partial x^2} + C_{66}^{(k)}\frac{\partial^2}{\partial y^2}\right)u_x^{(k)} + \left(C_{12}^{*(k)} + C_{66}^{(k)}\right)\frac{\partial^2 u_y^{(k)}}{\partial x\partial y} + \left(e_{11}^{*(k)}\frac{\partial^2}{\partial x^2} + e_{26}^{(k)}\frac{\partial^2}{\partial y^2}\right)\phi^{(k)} + \frac{C_{13}^{(k)}}{C_{33}^{(k)}}\frac{\partial\sigma_{zz}^{(k)}}{\partial x}\right] \\
\sigma_{yz,z}^{(k)} &= \rho\ddot{u}_y^{(k)} - \left[\left(C_{12}^{*(k)} + C_{66}^{(k)}\right)\frac{\partial^2 u_x^{(k)}}{\partial x\partial y} + \left(C_{66}^{(k)}\frac{\partial^2}{\partial x^2} + C_{22}^{*(k)}\frac{\partial^2}{\partial y^2}\right)u_y^{(k)} + \left(e_{12}^{*(k)} + e_{26}^{(k)}\right)\frac{\partial^2\phi^{(k)}}{\partial x\partial y} + \frac{C_{23}^{(k)}}{C_{33}^{(k)}}\frac{\partial\sigma_{zz}^{(k)}}{\partial y}\right] \\
d_{z,z}^{(k)} &= -\left[\left(e_{11}^{*(k)}\frac{\partial^2}{\partial x^2} + e_{26}^{(k)}\frac{\partial^2}{\partial y^2}\right)u_x^{(k)} + \left(e_{12}^{*(k)} + e_{26}^{(k)}\right)\frac{\partial^2 u_y^{(k)}}{\partial x\partial y} - \left(\epsilon_{11}^{*(k)}\frac{\partial^2}{\partial x^2} + \epsilon_{22}^{(k)}\frac{\partial^2}{\partial y^2}\right)\phi^{(k)} + \frac{e_{13}^{(k)}}{C_{33}^{(k)}}\frac{\partial\sigma_{zz}^{(k)}}{\partial x}\right]
\end{aligned}
\tag{5}
$$

The first three relations of Eq. (3) and the first one of Eq. (5) can be grouped into,

$$
\frac{\partial}{\partial z}\{x_1\}^{(k)} = [a_1]^{(k)}\{x_2\}^{(k)} \tag{6}
$$

where

$$
[a_1] = \begin{bmatrix} \frac{\epsilon_{33}}{\Delta_{35}} & 0 & \frac{e_{35}}{\Delta_{35}} & -\frac{\partial}{\partial x} \\ 0 & \frac{1}{C_{44}} & 0 & -\frac{\partial}{\partial y} \\ \frac{e_{35}}{\Delta_{35}} & 0 & -\frac{C_{55}}{\Delta_{35}} & 0 \\ -\frac{\partial}{\partial x} & -\frac{\partial}{\partial y} & 0 & \rho\frac{\partial^2}{\partial t^2} \end{bmatrix}, \quad \{x_2\} = \begin{Bmatrix} \sigma_{xz} \\ \sigma_{yz} \\ d_z \\ u_z \end{Bmatrix}
$$

The last relation of Eq. (3) and last three ones of Eq. (5) can be grouped into,

$$
\frac{\partial}{\partial z}\{x_2\}^{(k)} = [a_2]^{(k)}\{x_1\}^{(k)} \tag{7}
$$

where

$$
[a_2] = \begin{bmatrix} \rho\frac{\partial^2}{\partial t^2} - \left(C_{11}^*\frac{\partial^2}{\partial x^2} + C_{66}\frac{\partial^2}{\partial y^2}\right) & -\left(C_{12}^* + C_{66}\right)\frac{\partial^2}{\partial x\partial y} & -\left(e_{11}^*\frac{\partial^2}{\partial x^2} + e_{26}\frac{\partial^2}{\partial y^2}\right) & -\frac{C_{13}}{C_{33}}\frac{\partial}{\partial x} \\ -\left(C_{12}^* + C_{66}\right)\frac{\partial^2}{\partial x\partial y} & \rho\frac{\partial^2}{\partial t^2} - \left(C_{66}\frac{\partial^2}{\partial x^2} + C_{22}^*\frac{\partial^2}{\partial y^2}\right) & -\left(e_{12}^* + e_{26}\right)\frac{\partial^2}{\partial x\partial y} & -\frac{C_{23}}{C_{33}}\frac{\partial}{\partial y} \\ -\left(e_{11}^*\frac{\partial^2}{\partial x^2} + e_{26}\frac{\partial^2}{\partial y^2}\right) & -\left(e_{12}^* + e_{26}\right)\frac{\partial^2}{\partial x\partial y} & \epsilon_{11}^*\frac{\partial^2}{\partial x^2} + \epsilon_{22}\frac{\partial^2}{\partial y^2} & -\frac{e_{13}}{C_{33}}\frac{\partial}{\partial x} \\ -\frac{C_{13}}{C_{33}}\frac{\partial}{\partial x} & -\frac{C_{23}}{C_{33}}\frac{\partial}{\partial y} & -\frac{e_{13}}{C_{33}}\frac{\partial}{\partial x} & \frac{1}{C_{33}} \end{bmatrix}
$$

The combination of Eqs. (6) and (7) gives the kth piezoelectric lamina state space equation,

$$
\frac{\partial}{\partial z}\begin{Bmatrix} x_1 \\ x_2 \end{Bmatrix}^{(k)} = \begin{bmatrix} 0 & a_1 \\ a_2 & 0 \end{bmatrix}^{(k)}\begin{Bmatrix} x_1 \\ x_2 \end{Bmatrix}^{(k)} \tag{8a}
$$

$$
\frac{\partial}{\partial z}\{x\}^{(k)} = [a]^{(k)}\{x\}^{(k)} \tag{8b}
$$

Notice that the sub-matrices $[a_1]$ and $[a_2]$ of Eqs. 6,7,8a are individually symmetric thanks to the chosen order of the components of the state sub-vectors $\{x_1\}$ and $\{x_2\}$ but the lamina system matrix $[a]$ of Eq. (8b) is not symmetric.

3. Transfer matrices of simply-supported piezoelectric laminae

The plate is now considered SS so that transverse and tangential kth lamina displacements and normal stresses vanish at its vertical edges. Electrically, these are OC at $x = 0$, L_x and SC at $y = 0$, L_y, respectively. These conditions can be written as,

$$\sigma_{xx}^{(k)} = u_y^{(k)} = u_z^{(k)} = d_z^{(k)} = 0; \quad x = 0, L_x \tag{9a}$$

$$\sigma_{yy}^{(k)} = u_x^{(k)} = u_z^{(k)} = \phi^{(k)} = 0; \quad y = 0, L_y \tag{9b}$$

Primary mixed state variables that satisfy the electromechanical boundary conditions (9a) and (9b) can be written in trigonometric series as,

$$\begin{aligned}
(u_x, \sigma_{xz})^{(k)} &= (U_x(z), \Sigma_{xz}(z))^{(k)} \cos px \sin qy \exp \mathrm{i}\omega t \\
(u_y, \sigma_{yz})^{(k)} &= \left(U_y(z), \Sigma_{yz}(z)\right)^{(k)} \sin px \cos qy \exp \mathrm{i}\omega t \\
(u_z, \sigma_{zz})^{(k)} &= (U_z(z), \Sigma_{zz}(z))^{(k)} \sin px \sin qy \exp \mathrm{i}\omega t \\
(\phi, d_z)^{(k)} &= (\Phi(z), D_z(z))^{(k)} \cos px \sin qy \exp \mathrm{i}\omega t
\end{aligned} \tag{10}$$

From these, the secondary mixed state space variables take the forms,

$$\begin{aligned}
(\sigma_{xx}, \sigma_{yy}, d_x)^{(k)} &= \left(\Sigma_{xx}(z), \Sigma_{yy}(z), D_x(z)\right)^{(k)} \sin px \sin qy \exp \mathrm{i}\omega t \\
(\sigma_{xy}, d_y)^{(k)} &= \left(\Sigma_{xy}(z), D_y(z)\right)^{(k)} \cos px \cos qy \exp \mathrm{i}\omega t
\end{aligned} \tag{11}$$

In Eqs. (10) and (11), $\omega = \omega_{m_x m_y}$ is the circular frequency (rad/s), i is the imaginary unit ($i^2 = -1$), $p = m_x\pi/L_x$ and $q = m_y\pi/L_y$. The uppercase letters denote the amplitudes of the corresponding lowercase physical quantities.

It is worthwhile to notice that Fourier series of Eqs. (10) and (11) should be normally summed on m_x and m_y. Therefore, in the free-vibration analysis, it is well known that due to the orthogonal trigonometric functions and for orthotropic materials, these summations uncouple and the corresponding eigenvalue problem can be solved for each (m_x, m_y) couple.

The use of Eq. (11) in Eq. (4) transforms it to,

$$\{Y\}^{(k)} = [B]^{(k)} \{X_1\}^{(k)} \tag{12}$$

with

$$\{Y\} = \begin{Bmatrix} \Sigma_{xx} \\ \Sigma_{yy} \\ D_x \\ \Sigma_{xy} \\ D_y \end{Bmatrix}, \quad [B] = \begin{bmatrix} -C_{11}^* p & -C_{12}^* q & -e_{11}^* p & \frac{C_{13}}{C_{33}} \\ -C_{12}^* p & -C_{22}^* q & -e_{12}^* p & \frac{C_{23}}{C_{33}} \\ -e_{11}^* p & -e_{12}^* q & \epsilon_{11}^* p & \frac{e_{13}}{C_{33}} \\ C_{66} q & C_{66} p & e_{26} q & 0 \\ e_{26} q & e_{26} p & -\epsilon_{22} q & 0 \end{bmatrix}, \quad \{X_1\} = \begin{Bmatrix} U_x \\ U_y \\ \Phi \\ \Sigma_{zz} \end{Bmatrix}$$

Also, the substitution of Eq. (10) in the state space equation, Eq. (8), transforms it to,

$$\frac{\mathrm{d}}{\mathrm{d}z} \begin{Bmatrix} X_1 \\ X_2 \end{Bmatrix}^{(k)} = \begin{bmatrix} 0 & A_1 \\ A_2 & 0 \end{bmatrix}^{(k)} \begin{Bmatrix} X_1 \\ X_2 \end{Bmatrix}^{(k)} \quad \text{or} \quad \frac{\mathrm{d}}{\mathrm{d}z} \{X\}^{(k)} = [A]^{(k)} \{X\}^{(k)} \tag{13a,b}$$

where

$$\{X_2\} = \begin{Bmatrix} \Sigma_{xz} \\ \Sigma_{yz} \\ D_z \\ -U_z \end{Bmatrix}, \quad [A_1] = \begin{bmatrix} \frac{\epsilon_{33}}{\Delta_{35}} & 0 & \frac{e_{35}}{\Delta_{35}} & p \\ 0 & \frac{1}{C_{44}} & 0 & q \\ \frac{e_{35}}{\Delta_{35}} & 0 & -\frac{C_{55}}{\Delta_{35}} & 0 \\ p & q & 0 & -\rho\omega^2 \end{bmatrix},$$

$$[A_2] = \begin{bmatrix} -\rho\omega^2 + (C_{11}^* p^2 + C_{66} q^2) & (C_{12}^* + C_{66}) pq & e_{11}^* p^2 + e_{26} q^2 & -\frac{C_{13}}{C_{33}} p \\ (C_{12}^* + C_{66}) pq & -\rho\omega^2 + (C_{66} p^2 + C_{22}^* q^2) & (e_{12}^* + e_{26}) pq & -\frac{C_{23}}{C_{33}} q \\ e_{11}^* p^2 + e_{26} q^2 & (e_{12}^* + e_{26}) pq & -(\epsilon_{11}^* p^2 + \epsilon_{22} q^2) & -\frac{e_{13}}{C_{33}} p \\ -\frac{C_{13}}{C_{33}} p & -\frac{C_{23}}{C_{33}} q & -\frac{e_{13}}{C_{33}} p & -\frac{1}{C_{33}} \end{bmatrix}$$

The negative sign before the transverse mechanical displacement amplitude is introduced to keep symmetric the system bloc matrices.

Once Eq. (13b) is solved, Eq. (12) can be used, after extracting $\{X_1\}$, to compute the amplitudes of the in-plane stresses and electric displacements. The solution of Eq. (13b), for $z \in [z_k, z_{k+1}]$, can be written in the following transfer matrix form,

$$\{X(z)\}^{(k)} = [T(z - z_k)]^{(k)} \{X(z_k)\}^{(k)} \tag{14}$$

with

$$[T(z - z_k)]^{(k)} = \exp[(z - z_k)[A]^{(k)}]$$

$[T(z-z_k)]^{(k)}$ is the kth lamina transfer matrix which maps the state vector at its bottom surface with that at depth $z \in [z_k, z_{k+1}]$. The sate vector at the lamina top surface is then,

$$\{X(z_{k+1})\}^{(k)} = [T(h_k)]^{(k)} \{X(z_k)\}^{(k)} \tag{15}$$

where $h_k = z_{k+1} - z_k$ is the thickness of the kth lamina, and $[T(h_k)]^{(k)}$ its lamina transfer matrix which maps the state vector at its bottom surface to that at its top one. It is not symmetric, all full in contrary to the system matrix $[A]$, and of eighth order for a NE laminae. However, for electroded piezoelectric laminae the transfer matrix size can be reduced through analytic condensation of the electric state variables. The procedure is described hereafter but the readers are also encouraged to see the reference (Benjeddou and Deü, 2001a) for the static case.

3.1. Transfer matrix of an OC electroded inner piezoelectric lamina

An OC electroded piezoelectric lamina is considered here free of electric surface charge on its top and bottom surfaces; that is,

$$D_z^{(k)}(z_k) = D_z^{(k)}(z_{k+1}) = 0 \tag{16}$$

In this case, the electric potential at the lamina lower surface can be expressed from the 7th line of the linear system of Eq. (15), combined with the condition $D_z^{(k)}(z_{k+1}) = 0$, as,

$$\Phi^{(k)}(z_k) = \langle \overline{T}_{7j}(h_k); \quad j = 1, 2, 4\text{–}6, 8 \rangle^{(k)} \{\overline{X}(z_k)\}^{(k)} \tag{17}$$

where

$$\overline{T}_{7j}(h_k) = -\frac{T_{7j}(h_k)}{T_{73}(h_k)}; \quad j = 1, 2, 4\text{–}6, 8; \quad \langle \overline{X} \rangle = \langle U_x U_y \Sigma_{zz} \mid \Sigma_{xz} \Sigma_{yz} - U_z \rangle$$

The substitution of Eq. (17) and the electric condition $D_z^{(k)}(z_k) = 0$ in the 3rd and 7th lines of the system of Eq. (14) provides, respectively, the electric potential and displacement inside the kth OC piezoelectric lamina,

$$\Phi^{(k)}(z) = \left\langle \overline{T}_{3j}(z - z_k); j = 1, 2, 4\text{–}6, 8 \right\rangle^{(k)} \{\overline{X}(z_k)\}^{(k)} \tag{18a}$$

$$D_z^{(k)}(z) = \left\langle \overline{T}_{7j}(z - z_k); j = 1, 2, 4\text{–}6, 8 \right\rangle^{(k)} \{\overline{X}(z_k)\}^{(k)} \tag{18b}$$

with

$$\overline{T}_{ij}(z - z_k) = T_{ij}(z - z_k) - T_{i3}(z - z_k)\frac{T_{7j}(h_k)}{T_{73}(h_k)}; \quad i = 3, 7;\ j = 1, 2, 4\text{–}6, 8$$

Finally, the substitution of Eq. (17) and the condition $D_z^{(k)}(z_k) = 0$ in the other than 3rd and 7th lines of the system given by Eq. (14) reduces it to the following *sixth order* one,

$$\{\overline{X}(z)\}^{(k)} = \left[\overline{T}(z - z_k)\right]^{(k)} \{\overline{X}(z_k)\}^{(k)} \tag{19}$$

where the matrix components are as after Eq. (18b) but with $i = 1,2,4\text{–}6,8$. This equation can be used to evaluate the mechanical displacements and transverse stresses at $z = z_{k+1}$; i.e.,

$$\{\overline{X}(z_{k+1})\}^{(k)} = [\overline{\overline{T}}(h_k)]^{(k)} \{\overline{X}(z_k)\}^{(k)} \tag{20}$$

where $[\overline{T}(h_k)]^{(k)}$ is the transfer matrix of the kth OC electrode inner piezoelectric lamina.

3.2. Transfer matrix of a SC electroded inner piezoelectric lamina

A SC electroded piezoelectric lamina is considered here free of electric potential on its top and bottom surfaces; that is,

$$\Phi^{(k)}(z_k) = \Phi^{(k)}(z_{k+1}) = 0 \tag{21}$$

In this case, the transverse electric displacement at the lamina lower surface can be expressed from the 3rd line of the linear system of Eq. (15) and using $\Phi^{(k)}(z_{k+1}) = 0$, as,

$$D_z^{(k)}(z_k) = \left\langle \overline{\overline{T}}_{3j}(h_k); j = 1, 2, 4 - 6, 8 \right\rangle^{(k)} \{\overline{X}(z_k)\}^{(k)} \tag{22}$$

with

$$\overline{\overline{T}}_{3j}(h_k) = -\frac{T_{3j}(h_k)}{T_{37}(h_k)}; \quad j = 1, 2, 4 - 6, 8$$

The substitution of Eq. (22) and $\Phi^{(k)}(z_k) = 0$ in the 7th and 3rd lines of the system of Eq. (14) provides, respectively, the transverse electric displacement and potential inside the kth SC piezoelectric lamina,

$$D_z^{(k)}(z) = \left\langle \overline{\overline{T}}_{7j}(z - z_k); j = 1, 2, 4 - 6, 8 \right\rangle^{(k)} \{\overline{X}(z_k)\}^{(k)} \tag{23a}$$

$$\Phi^{(k)}(z) = \left\langle \overline{\overline{T}}_{3j}(z - z_k); j = 1, 2, 4 - 6, 8 \right\rangle^{(k)} \{\overline{X}(z_k)\}^{(k)} \tag{23b}$$

with

$$\overline{\overline{T}}_{ij}(z - z_k) = T_{ij}(z - z_k) - T_{i7}(z - z_k)\frac{T_{3j}(h_k)}{T_{37}(h_k)}; \quad i = 7, 3;\ j = 1, 2, 4\text{–}6, 8$$

Finally, the substitution of Eq. (22) and the condition $\Phi^{(k)}(z_k) = 0$ in the other-than 3rd and 7th lines of the system given by Eq. (14) reduces it to the following *sixth order* one,

$$\{\overline{X}(z)\}^{(k)} = \left[\overline{T}(z - z_k)\right]^{(k)} \{\overline{X}(z_k)\}^{(k)} \tag{24}$$

where the matrix components are as after Eq. (23b) but with $i = 1,2,4–6,8$. This equation can be used to evaluate the mechanical displacements and transverse stresses at $z = z_{k+1}$; i.e.,

$$\{\overline{X}(z_{k+1})\}^{(k)} = \left[\overline{\overline{T}}(h_k)\right]^{(k)} \{\overline{X}(z_k)\}^{(k)} \tag{25}$$

where $[\overline{\overline{T}}(h_k)]^{(k)}$ is the transfer matrix of the kth SC electrode inner piezoelectric lamina.

3.3. Case of an elastic lamina

An elastic layer is considered piezoelectric with nil coupling constants ($e_{ij} = 0$). It needs no special treatment of its transfer matrix. However, the following interesting special features regarding the electric state in a *conducting* elastic lamina can be emphasized:

As expected, an electromechanical *uncoupling* occurs for an elastic layer. This is due to the fact that, in the 3rd and 7th lines and columns of Eq. (13b), the only non-vanishing terms are A_{37} and A_{73} so that the following dielectric state space equation holds in the kth elastic layer,

$$\frac{\mathrm{d}}{\mathrm{d}z}\begin{Bmatrix} \Phi(z) \\ D_z(z) \end{Bmatrix}^{(k)} = \begin{bmatrix} 0 & A_{37} \\ A_{73} & 0 \end{bmatrix}^{(k)} \begin{Bmatrix} \Phi(z) \\ D_z(z) \end{Bmatrix}^{(k)} \tag{26}$$

with

$$A_{37} = -\frac{1}{\epsilon_{33}}, \quad A_{73} = -(\epsilon_{11}p^2 + \epsilon_{22}q^2)$$

Following the procedure proposed by Bahar (1977), the solution of Eq. (26) is,

$$\begin{Bmatrix} \Phi(z) \\ D_z(z) \end{Bmatrix}^{(k)} = \begin{bmatrix} T_{33}(z - z_k) & T_{37}(z - z_k) \\ T_{73}(z - z_k) & T_{77}(z - z_k) \end{bmatrix}^{(k)} \begin{Bmatrix} \Phi(z_k) \\ D_z(z_k) \end{Bmatrix}^{(k)} \tag{27}$$

with

$$T_{33}(z - z_k) = T_{77}(z - z_k) = \cosh\left[(z - z_k)\sqrt{\frac{\epsilon_{11}p^2 + \epsilon_{22}q^2}{\epsilon_{33}}}\right]$$

$$T_{37}(z - z_k) = -\frac{1}{\sqrt{\epsilon_{33}(\epsilon_{11}p^2 + \epsilon_{22}q^2)}} \sinh\left[(z - z_k)\sqrt{\frac{\epsilon_{11}p^2 + \epsilon_{22}q^2}{\epsilon_{33}}}\right]$$

$$T_{73}(z - z_k) = -\sqrt{\epsilon_{33}(\epsilon_{11}p^2 + \epsilon_{22}q^2)} \sinh\left[(z - z_k)\sqrt{\frac{\epsilon_{11}p^2 + \epsilon_{22}q^2}{\epsilon_{33}}}\right]$$

Written for the top surface of the kth elastic lamina, Eq. (27) reads,

$$\begin{Bmatrix} \Phi(z_{k+1}) \\ D_z(z_{k+1}) \end{Bmatrix}^{(k)} = \begin{bmatrix} T_{33}(h_k) & T_{37}(h_k) \\ T_{73}(h_k) & T_{77}(h_k) \end{bmatrix}^{(k)} \begin{Bmatrix} \Phi(z_k) \\ D_z(z_k) \end{Bmatrix}^{(k)} \tag{28}$$

From Eq. (22), the in-plane electric displacements inside an elastic lamina are,

$$\left\{ \begin{array}{c} D_x(z-z_k) \\ D_y(z-z_k) \end{array} \right\}^{(k)} = \left\{ \begin{array}{c} \epsilon_{11} p \\ -\epsilon_{22} q \end{array} \right\}^{(k)} \Phi^{(k)}(z-z_k) \tag{29}$$

Hence, either of the in-plane electric displacements vanishes when p or q is nil. However, both vanish independently of the mode order when the electric potential is nil. This happens, for example, for SC electrodes.

Eqs. (27) and (29) define the whole electric state inside an elastic *conducting* lamina, whereas, Eq. (28) can be used to compute interface electric transverse displacement and electric potential.

As a consequence of the previous point, the remaining part of an elastic lamina transfer matrix, i.e. without the 3rd and 7th lines and columns, is identical to both transfer matrices of OC, Eq. (20), and SC, Eq. (25), electroded piezoelectric lamina but with nil coupling constants, as mentioned above.

4. Free-vibration problems of SS piezoelectric laminated plates

For a free-vibration analysis, the top and bottom plate surfaces are here non-electroded and unloaded. The mechanical and electric boundary conditions on these surfaces are then,

$$\Sigma_{iz}^{(1)}(0) = \Sigma_{iz}^{(N)}(H) = 0, \quad i = x, y, z \tag{30}$$

$$D_z^{(1)}(0) = D_z^{(N)}(H) = 0 \tag{31}$$

The eigenvalue problem to be solved for the free-vibration analysis is obtained by the assembly of the laminae transfer matrices using the interlayer interface continuity conditions which depend on the assumed mechanical and electric bonding conditions (i.e., the presence or not of inner electrodes). However, perfect mechanical bonding is assumed for all interfaces. That is, the mechanical displacements and transverse stresses are considered continuous across the interface between (k) and (k+1) layers,

$$U_i^{(k)}(z_{k+1}) = U_i^{(k+1)}(z_{k+1}), \quad i = x, y, z; \ k = 1, \ldots, N-1 \tag{32}$$

$$\Sigma_{iz}^{(k)}(z_{k+1}) = \Sigma_{iz}^{(k+1)}(z_{k+1}), \quad i = x, y, z; \ k = 1, \ldots, N-1 \tag{33}$$

These interface conditions can be written in term of the reduced state space vector, introduced in Eq. (17), as,

$$\{\overline{X}(z_{k+1})\}^{(k+1)} = \{\overline{X}(z_{k+1})\}^{(k)}, \quad k = 1, \ldots, N-1 \tag{34}$$

4.1. Assembly with non-electroded inner piezoelectric layers

For a NE inner piezoelectric lamina, electric transverse displacement and potential are considered continuous across the interface between (k) and ($k+1$), so that the piezoelectric layers can be seen as electrically perfectly bonded,

$$\Phi^{(k)}(z_{k+1}) = \Phi^{(k+1)}(z_{k+1}), \quad k = 1, \ldots, N-1 \tag{35}$$

$$D_z^{(k)}(z_{k+1}) = D_z^{(k+1)}(z_{k+1}), \quad k = 1, \ldots, N-1 \tag{36}$$

Hence, in this case, mechanical and electric perfect bonding conditions can be assumed. This means that all electromechanical interface continuity relations, Eqs. (32), (33), (35), (36) hold. These can also be written in term of the full state vector, introduced in Eq. (13b),

$$\{X(z_{k+1})\}^{(k+1)} = \{X(z_{k+1})\}^{(k)}, \quad k = 1, \ldots, N-1 \tag{37}$$

Using recursively Eq. (37), combined with Eq. (15), provides an 8th *order* assembled transfer matrix equation,

$$\{X(H)\} = [T(H)]\{X(0)\} \tag{38}$$

with

$$[T(H)] = \prod_{k=N}^{1} [T(h_k)]$$

the so-called *plate transfer matrix* which is the product of the laminae transfer matrices.

Eq. (38) can be partitioned, after suitable rows and columns interchanges, so that,

$$\begin{Bmatrix} X_U(H) \\ X_\Sigma(H) \end{Bmatrix} = \begin{bmatrix} T_{UU}(H) & T_{U\Sigma}(H) \\ T_{\Sigma U}(H) & T_{\Sigma\Sigma}(H) \end{bmatrix} \begin{Bmatrix} X_U(0) \\ X_\Sigma(0) \end{Bmatrix} \tag{39}$$

where

$$\langle X_U \rangle = \langle\, U_x \quad U_y \quad -U_z \quad \Phi \,\rangle, \quad \langle X_\Sigma \rangle = \langle\, \Sigma_{xz} \quad \Sigma_{yz} \quad \Sigma_{zz} \quad D_z \,\rangle.$$

Since, the plate bottom and top surfaces are also NE (free of transverse stresses and electric displacement), Eqs. (30) and (31) lead to the following relations,

$$\{X_\Sigma(0)\} = \{X_\Sigma(H)\} = \{0\} \tag{40}$$

which, when used in Eq. (39), give the following *fourth order* only free-vibration problem,

$$[T_{\Sigma U}(H)]\{X_U(0)\} = \{0\} \tag{41}$$

4.2. Assembly with electroded inner piezoelectric layers

For an electroded inner piezoelectric lamina, the interfaces could be either SC or OC so that the corresponding EBC are given by Eqs. (16) and (21), respectively. Here, because of the *conducting* electrodes, either of the constraints of Eqs. (35) or (36) has to be relaxed when the dual state variable is known in order to allow for discontinuous electric transverse displacement for SC electrodes, or discontinuous electric potential for OC ones. This is obtained here *automatically* (see the results in the validation section), i.e. without implementing either of Eqs. (35) and (36), thanks to the *analytical condensation* of the electric state variables at the piezoelectric lamina transfer matrix level (see the previous section). Besides, this condensation procedure has made possible to reduce the 8th *order* transfer matrix systems of Eqs. (14) and (15), respectively, to those of 6th *order* only given by Eqs. (19) and (20) for OC electroded inner piezoelectric laminae, and by Eqs. (24) and (25) for the SC case. Eqs. (20) and (25) can be also written in the following *unified form*,

$$\{\overline{X}(z_{k+1})\}^{(k)} = \left[\widehat{T}(h_k)\right]^{(k)} \{\overline{X}(z_k)\}^{(k)} \tag{42}$$

where $[\widehat{T}(h_k)]^{(k)}$ is $[\overline{T}(h_k)]^{(k)}$ for the OC case and $[\overline{\overline{T}}(h_k)]^{(k)}$ for the SC one. Eq. (42) can then be used recursively, together with Eq. (34), to get,

$$\{\overline{X}(H)\} = \left[\widehat{T}(H)\right]\{\overline{X}(0)\} \tag{43}$$

with

$$\left[\widehat{T}(H)\right] = \prod_{k=N}^{1} \left[\widehat{T}(h_k)\right]$$

the laminate (assembled) transfer matrix.

After interchanging suitably its rows and columns, Eq. (43) can be partitioned so that,

$$\begin{Bmatrix} \overline{X}_U(H) \\ \overline{X}_\Sigma(H) \end{Bmatrix} = \begin{bmatrix} \widehat{T}_{UU}(H) & \widehat{T}_{U\Sigma}(H) \\ \widehat{T}_{\Sigma U}(H) & \widehat{T}_{\Sigma\Sigma}(H) \end{bmatrix} \begin{Bmatrix} \overline{X}_U(0) \\ \overline{X}_\Sigma(0) \end{Bmatrix} \tag{44}$$

where

$$\langle \overline{X}_U \rangle = \langle\, U_x \quad U_y \quad -U_z \,\rangle, \quad \langle \overline{X}_\Sigma \rangle = \langle\, \Sigma_{xz} \quad \Sigma_{yz} \quad \Sigma_{zz} \,\rangle$$

Since the plate bottom and top surfaces are stress-free, then Eq. (30) leads to,

$$\{\overline{X}_\Sigma(0)\} = \{\overline{X}_\Sigma(H)\} = \{0\} \tag{45}$$

which, when substituted in Eq. (44), give the following *third order* free-vibration problem,

$$\left[\widehat{T}_{\Sigma U}(H)\right]\{\overline{X}_U(0)\} = \{0\} \tag{46}$$

5. Implementation and computational aspects

The present 3D mixed state space formulation can be implemented via these main steps:

- Construct the system matrices $[A]^{(k)}$, Eqs. (13a,b), and $[B]^{(k)}$, Eq. (12), for the N laminae.
- Compute the laminae transfer matrices for the considered major surfaces boundary conditions; i.e., $[T(h_k)]^{(k)}$, Eq. (15), for NE, $[\overline{T}(h_k)]^{(k)}$, Eq. (20), for OC or $\left[\overline{\overline{T}}(h_k)\right]^{(k)}$, Eq. (25), for SC laminae.
- Construct the plate transfer matrix for the considered lamination scheme; that is, $[(T\ H)]$, Eq. (38), for NE or $\left[\widehat{T}(H)\right]$, Eq. (43), for electroded laminate.
- Solve the free-vibration problem of 4th order, Eq. (41), for perfectly bonded laminate or of 3rd order, Eq. (46), for a laminate with embedded electroded piezoelectric layers.
- Evaluate the interface unknowns using Eq. (15) for a NE interface or Eqs. (20) and (25) for OC/SC electroded interfaces, respectively.
- For the electroded piezoelectric laminae, calculate at the layer bottom surfaces the electric potential for OC laminae using Eq. (17) or the transverse electric displacement for SC laminae using Eq. (22).
- Once previous quantities are computed for all the layers, the through-the-thickness distributions of the electromechanical state variables can be calculated using Eq. (14).

In the current implementation, no effort has been made to optimize the calculations of the laminae transfer matrices or their products during their assemblage. All matrix manipulations have been let to the expertise of the MATLAB® software. The latter was also used to solve numerically the characteristic equations (41) and (46), for several values of ω in a given frequency range. Once, a change of sign is found for the determinant, the bisection method is used to refine the root estimation to the required accuracy (see Fig. 2). It is worthy also to recall that, for fixed (m_x, m_y), an infinite number of solutions exist for Eqs. (41) and (46) representing the so-called *thickness modes*. For each calculated natural frequency, the initial displacement amplitudes are computed using these equations and the reduced state vector is reconstructed, then the interfaces unknowns are deduced from Eqs. (15) and (42). After that, the thickness distributions of the electromechanical sate variables are calculated from Eqs. (14), (19) and (24) for a given EBC (NE, OC or SC).

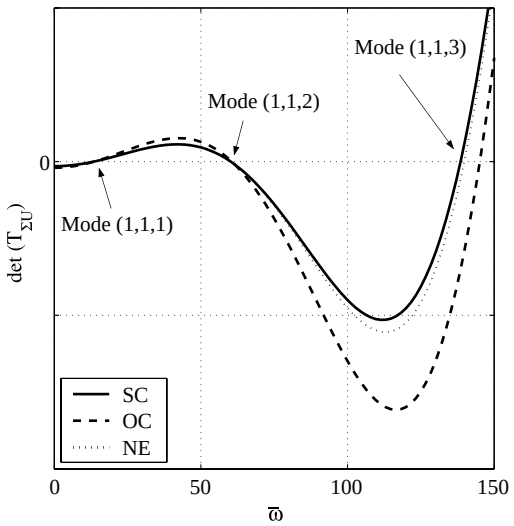

Fig. 2. Solution of the characteristic equation for different EBC (SC, OC, NE).

6. Some expected results and validation

Since the free-vibration of SS laminated plates with embedded shear-mode piezoceramic layers is analyzed for the first time here, there are no reference results in the open literature except those presented earlier by the authors (Deü and Benjeddou, 2002; Benjeddou and Deü, 2003). Thus, for the validation of the proposed exact 3D solution, some expected results are first demonstrated for a sandwich plate with *x-poled* piezoceramic core and *conducting* elastic faces, and for the *special* ($m_x = 0$ or $m_y = 0$) modes; Then, the obtained results are taken as reference for those computed with the MSSA.

6.1. Expected results for a SS sandwich plate with shear-mode piezoceramic core

As shown above, an electromechanical uncoupling occurs for an elastic lamina. Thus, the resulting dielectric transfer matrix equation, Eq. (28), can be used for the calculation of the electric state variables at top/bottom surfaces of the lamina and their distributions at its depth z can be recovered using Eq. (27).

Lets now try to get more precise ideas on these distributions for the different EBC at the upper/lower surfaces of an elastic layer. The different situations considered here are shown in Fig. 3 for a sandwich plate with shear-mode (*x-poled*) core and *conducting* elastic faces.

Consider first the SC configuration (Fig. 3a) for which the EBC at the lower and upper surfaces of the bottom ($k = 1$) conducting elastic face are,

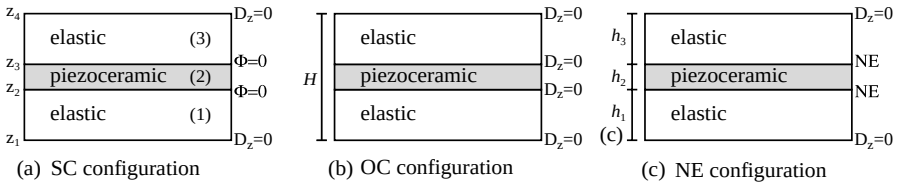

Fig. 3. A sandwich plate with SC/OC electroded or NE shear-mode piezoceramic core.

$$D_z^{(1)}(z_1) = 0, \quad \Phi^{(1)}(z_2) = 0 \tag{47}$$

Substituting back these relations in Eq. (28) gives,

$$\Phi^{(1)}(z_1) = 0, \quad D_z^{(1)}(z_2) = 0 \tag{48}$$

Now, introducing the first relations of Eqs. (47) and (48) into Eq. (27), provides,

$$\Phi^{(1)}(z) = 0, \quad D_z^{(1)}(z) = 0 \tag{49}$$

These relations prove that the electric state variables are nil inside the SC bottom conducting elastic face of the sandwich shear-mode adaptive SS plate.

The EBC on the lower and upper surfaces of the top ($k = 3$) conducting elastic face are,

$$\Phi^{(3)}(z_3) = 0, \quad D_z^{(3)}(z_4) = 0 \tag{50}$$

When substituted back in Eq. (28) these relations provide,

$$D_z^{(3)}(z_3) = 0, \quad \Phi^{(3)}(z_4) = 0 \tag{51}$$

Combining the first relations of Eqs. (50) and (51) into Eq. (27), gives,

$$\Phi^{(3)}(z) = 0, \quad D_z^{(3)}(z) = 0 \tag{52}$$

This equation proves that the electric state variables are also nil inside the SC top conducting elastic face of the sandwich shear-mode adaptive SS plate.

The transverse electric displacement and electric potential inside the SC piezoceramic core ($k = 2$) are given, respectively, by Eqs. (23a) and (23b). From them, it can be shown that the EBC at the lower and upper surfaces of the piezoceramic core are, respectively,

$$\Phi^{(2)}(z_2) = 0, \quad D_z^{(2)}(z_2) = \left\langle \overline{\overline{T}}_{7j}(0); j = 1,2,4\text{–}6,8 \right\rangle^{(2)} \left\{ \overline{X}(z_2) \right\}^{(2)} \tag{53}$$

$$\Phi^{(2)}(z_3) = 0, \quad D_z^{(2)}(z_3) = \left\langle \overline{\overline{T}}_{7j}(h_k); j = 1,2,4\text{–}6,8 \right\rangle^{(2)} \left\{ \overline{X}(z_2) \right\}^{(2)} \tag{54}$$

Combining the last relations of Eqs. (47) and (48), the first ones of Eqs. (50) and (51) and Eqs. (53) and (54) provides the electric interface conditions at the lower (z_2) and upper (z_3) interfaces,

$$\Phi^{(1)}(z_2) = \Phi^{(2)}(z_2), \quad D_z^{(1)}(z_2) \neq D_z^{(2)}(z_2) \tag{55}$$

$$\Phi^{(2)}(z_3) = \Phi^{(3)}(z_3), \quad D_z^{(2)}(z_3) \neq D_z^{(3)}(z_3) \tag{56}$$

These relations indicate that, for the SC configuration, the *electric potential is continuous* at the interfaces whereas, the *transverse electric displacement is discontinuous*.

The same previous procedure (see also Benjeddou and Deü, 2001b) can be followed for the OC configuration (Fig. 3b) to demonstrate that, in this case, the opposite situation occurs,

$$D_z^{(1)}(z_2) = D_z^{(2)}(z_2), \quad \Phi^{(1)}(z_2) \neq \Phi^{(2)}(z_2) \tag{57}$$

$$D_z^{(2)}(z_3) = D_z^{(3)}(z_3), \quad \Phi^{(2)}(z_3) \neq \Phi^{(3)}(z_3) \tag{58}$$

Hence, for the OC configuration, the *electric potential is discontinuous* at the interfaces whereas, the *transverse electric displacement is continuous*. Regarding the in-plane electric displacements, Eq. (29), together with the first relations of Eqs. (49) and (52), indicate that they vanish, independently of the mode order, in the elastic faces with SC/OC interfaces.

In summary, the electric state variables are nil in the conducting elastic faces of a SS sandwich plate with SC or OC electroded shear-mode piezoceramic core. Also, the electric state variable corresponding to the known (SC or OC) one is continuous at the sandwich interfaces; whereas, the dual one is discontinuous at the same interfaces. These results generalize, to the free-vibration of a sandwich SS plate with a shear-mode piezoceramic core, those demonstrated for the static actuation and sensing of the same adaptive sandwich plate (Benjeddou and Deü, 2001b).

It is worthy to notice that OC EBC on top/bottom plate can be seen also as NE ones. Besides, although often considered in the literature, inner NE piezoceramic laminae are in fact useless in practice since they have to be electroded when used as sensors/actuators.

6.2. Special ($m_x = 0$ or $m_y = 0$) modes

As mentioned in Batra and Aimmanee (2003), the special modes for either $m_x = 0$ or $m_y = 0$ were often missed by most exact or analytical solutions. For piezoelectric plates, these were mentioned briefly and only for extension-mode piezoelectric materials, first in Ding et al. (2000) and then in the former reference. It is then worthy to analyze and discuss here for the first time these special modes for the shear-mode piezoceramic materials.

For $m_x = 0$, the exact solution of the kth lamina provides the following *only non-nil* primary state variables (Eq. (10) with $p = 0$),

$$\begin{aligned}(u_x, \sigma_{xz})^{(k)} &= (U_x(z), \Sigma_{xz}(z))^{(k)} \sin qy \exp \mathrm{i}\omega t \\ (\phi, d_z)^{(k)} &= (\Phi(z), D_z(z))^{(k)} \sin qy \exp \mathrm{i}\omega t\end{aligned} \tag{59}$$

and *only non-nil* secondary state variables (Eq. (11) with $p = 0$),

$$(\sigma_{xy}, d_y)^{(k)} = \left(\Sigma_{xy}(z), D_y(z)\right)^{(k)} \cos qy \exp \mathrm{i}\omega t \tag{60}$$

The mixed state space equations reduce then to (Eq. (13a) with $p = 0$),

$$\frac{\mathrm{d}}{\mathrm{d}z}\begin{Bmatrix} U_x \\ \Phi \end{Bmatrix}^{(k)} = \frac{1}{\Delta_{35}^{(k)}}\begin{bmatrix} \epsilon_{33} & e_{35} \\ e_{35} & -C_{55} \end{bmatrix}^{(k)} \begin{Bmatrix} \Sigma_{xz} \\ D_z \end{Bmatrix}^{(k)} \tag{61}$$

and

$$\frac{\mathrm{d}}{\mathrm{d}z}\begin{Bmatrix} \Sigma_{xz} \\ D_z \end{Bmatrix}^{(k)} = \begin{bmatrix} -\rho\omega^2 + C_{66}q^2 & e_{26}q \\ e_{26}q & -\epsilon_{22}q^2 \end{bmatrix}^{(k)} \begin{Bmatrix} U_x \\ \Phi \end{Bmatrix}^{(k)} \tag{62}$$

while the only non-nil secondary sate variables are (Eq. (12) with $p = 0$),

$$\begin{Bmatrix} \Sigma_{xy} \\ D_y \end{Bmatrix}^{(k)} = q\begin{bmatrix} C_{66} & e_{26} \\ e_{26} & -\epsilon_{22} \end{bmatrix}^{(k)} \begin{Bmatrix} U_x \\ \Phi \end{Bmatrix}^{(k)} \tag{63}$$

Eqs. (59)–(63) show clearly that, in contrary to the extension-mode piezoelectric materials (Batra and Aimmanee, 2003), the shear-mode ones render the special modes corresponding to $m_x = 0$ *coupled*. In particular, they couple the x–z transverse shear stress to the transverse electric displacement via the e_{35} shear piezoelectric constant, and the mechanical x-displacement to the electric potential via the e_{26} shear piezoelectric constant. Another important result shown by above equations is that, also in contrary to what has been mentioned in Batra and Aimmanee (2003), these modes are not pure in-plane torsion modes but are *combined in plane and $x - z$ transverse shear* modes.

Similarly, lets now consider the case of $m_y = 0$ for which the *only non-nil* primary state variables are (Eq. (10) with $q = 0$),

$$(u_y, \sigma_{yz})^{(k)} = \left(U_y(z),\ \Sigma_{yz}(z)\right)^{(k)} \sin px \exp \mathrm{i}\omega t \tag{64}$$

while the *only non-nil* secondary state variables are (Eq. (11) with $q = 0$),

$$(\sigma_{xy}, d_y)^{(k)} = \left(\Sigma_{xy}(z), D_y(z)\right)^{(k)} \cos px \exp \mathrm{i}\omega t \tag{65}$$

The mixed state space equations reduce then to (Eq. (13a) with $q = 0$),

$$\frac{\mathrm{d}}{\mathrm{d}z}\begin{Bmatrix} U_y \\ \Sigma_{yz} \end{Bmatrix}^{(k)} = \begin{bmatrix} 0 & \frac{1}{C_{44}} \\ -\rho\omega^2 + C_{66}p^2 & 0 \end{bmatrix}^{(k)} \begin{Bmatrix} U_y \\ \Sigma_{yz} \end{Bmatrix}^{(k)} \tag{66}$$

and the only non-vanishing secondary sate variables are (Eq. (12) with $q = 0$),

$$\begin{Bmatrix} \Sigma_{xy} \\ D_y \end{Bmatrix}^{(k)} = p \begin{Bmatrix} C_{66} \\ e_{26} \end{Bmatrix}^{(k)} U_y^{(k)} \tag{67}$$

Eqs. (64)–(67) show clearly that, in contrary to the special $m_x = 0$ modes, those corresponding to $m_y = 0$ are *uncoupled*. Again, above equations show also that these modes are not pure in-plane torsional modes, as mentioned in Batra and Aimmanee (2003), but are *combined in plane and $y-z$ transverse shear* modes. An additional important result is that (see Eq. (67)), in contrary to the previous modes, here the electric y-displacement is only due to the coupling with the corresponding mechanical displacement component; thus, it is nil in a conducting elastic lamina for which the e_{26} constant vanishes.

Regarding the in-plane electric displacements distributions for the two types of special modes, it was shown above that they are nil for the SC/OC sandwich configurations for all modes. However, for the NE case, only the y-displacement of the coupled special $m_x = 0$ modes is expected to be non-nil in the elastic faces as can be seen from Eqs. (29) and (63).

In summary, the special $m_x = 0$ modes are coupled whereas those corresponding to $m_y = 0$ are *uncoupled*. Besides, the in-plane electric displacements of these modes are nil in the elastic faces with SC/OC electroded interfaces. However, only the electric y-displacement is non-nil for the coupled special $m_x = 0$ modes of the NE configuration.

It is worthy to notice that the special ($m_x = 0$ or $m_y = 0$) modes are of theoretical and numerical interests only, for validation purpose for example. They exist only for some particular mechanical edge boundary conditions which are useless in smart structures.

6.3. Exact 3D mixed state space solution results

Above expected theoretical results are considered here as reference for the validation of the proposed exact 3D MSSA. For this, a *basic configuration*, consisting of a SS square sandwich plate with total thickness $H = 1$ cm and side-to-thickness ratio $L/H = 10$, is considered. Its faces, of thickness $0.4H$ each, are made of a 0° Graphite–Epoxy (GE) composite material, whereas its $0.2H$-thick core is constituted of an x-poled PZT-5H piezoceramic material (Fig. 3). The different material properties are given in Table 1.

The analysis of the results is made using the following *non-dimensional* frequency,

$$\varpi = \omega \frac{L^2}{H}\sqrt{\frac{\rho^{(c)}}{C_{55}^{(c)}}} \tag{68}$$

and *non-dimensional* electromechanical state variables (superscript c states for the core),

$$U_i^* = \frac{1}{U^{\max}} U_i, \quad \Sigma_{ij}^* = \frac{L}{C_{55}^{(c)} U^{\max}} \Sigma_{ij}, \quad D_i^* = \frac{L}{e_{35}^{(c)} U^{\max}} D_i, \quad \Phi^* = \frac{e_{35}^{(c)}}{C_{55}^{(c)} U^{\max}} \Phi \tag{69}$$

Table 1
Properties of the graphite–epoxy and shear-mode PZT-5H materials

Properties	Graphite–Epoxy	x-poled PZT-5H
C_{11} (GPa)	183.443	117
C_{22} (GPa)	11.662	126
C_{33} (GPa)	11.662	126
C_{12} (GPa)	4.363	84.1
C_{13} (GPa)	4.363	84.1
C_{23} (GPa)	3.918	79.5
C_{44} (GPa)	2.870	23
C_{55} (GPa)	2.870	23
C_{66} (GPa)	7.170	23
e_{11} (Cm^{-2})	0	23.3
e_{12} (Cm^{-2})	0	−6.5
e_{13} (Cm^{-2})	0	−6.5
e_{26} (Cm^{-2})	0	17
e_{35} (Cm^{-2})	0	17
ϵ_{11} ($10^{-10}\ \mathrm{Fm}^{-1}$)	153	130
ϵ_{22} ($10^{-10}\ \mathrm{Fm}^{-1}$)	153	150.3
ϵ_{33} ($10^{-10}\ \mathrm{Fm}^{-1}$)	153	150.3
ρ (kgm^{-3})	1580	7500

In contrary to the widespread practice of the mechanical researchers community, the small differences between SC and OC natural frequencies are not neglected but used to evaluate the *effective modal* EMCC (Rogacheva, 1994). Its square represents physically the percentage of the mechanical strain energy converted into the electric one and vice versa,

$$\mathrm{EMCC}(\%) = 100 \times \sqrt{\frac{\omega_{\mathrm{OC}}^2 - \omega_{\mathrm{SC}}^2}{\omega_{\mathrm{OC}}^2}} \tag{70}$$

The first *fifty* modes of the above basic configuration were extracted using the proposed MSSA for the full elastic (EL) and hybrid sandwich plates with either NE or SC/OC electroded piezoceramic core (Fig. 3). Pure elastic modes have been also computed with the FE code MSC-NASTRAN® to check the modes identification.

The obtained results are shown in Table 2, for the non-dimensional frequencies and EMMC, and in Fig. 4 for the first 15 modal shapes. They indicate that,

- The MSSA EL results much very well those obtained with 3D FE. The latter were obtained within a maximum error of 1.14% with a mesh of $50 \times 50 \times 5$ elements. Notice the changes of appearance order of some modes higher than the 27th one (see *italic* numbers of the 2nd and 3rd columns of Table 2). A finer mesh of $100 \times 100 \times 10$ elements has reduced the maximum error to only 0.29 % but has not eliminated the changes of the appearance order of the above higher modes.
- The SC non-dimensional frequencies differ only very slightly from those of the full EL plate, whereas, those of the sandwich plate with NE piezoceramic core are very close to those of the sandwich plate with OC electroded piezoceramic core.
- Each of the four couples of *special* modes, ($m_x = 1$–4, 0, 2) and ($0, m_y = 1$–4, 2), present in the computed first fifty modes, has almost the same non-dimensional frequencies, as mentioned in Batra and Aimmanee (2003) for EL and SC extension-mode piezoelectric materials. However, this is not true here for the OC EBC. Besides, as expected from the above section, ($m_x = 1$–4, 0, 2) modes are *uncoupled*

Table 2
First fifty non-dimensional frequencies of SS elastic and shear-mode adaptive sandwich plates

Mode			Elastic (EL) sandwich plate			Shear-mode adaptive sandwich plate			
$(m_x m_y m_z)$	No. (FE)	No. (MSSA)	MSSA	3D FE ($50\times50\times5$)	Error (%)	SC core	OC core	NE core	EMCC (%)
(1,1,1)	1	1	13.492	13.524	0.24	13.492	13.558	13.558	9.92
(1,2,1)	2	2	19.770	19.794	0.12	19.770	19.839	19.838	8.28
(1,3,1)	3	3	31.733	31.772	0.12	31.733	31.800	31.799	6.50
(1,0,2)	4	4	**34.688**	**34.682**	−0.02	**34.688**	**34.688**	34.688	**0.00**
(0,1,2)	5	5	**34.690**	**34.684**	−0.02	**34.692**	**40.635**	35.947	**52.07**
(2,1,1)	6	6	40.678	40.994	0.78	40.678	41.257	41.251	16.69
(2,2,1)	7	7	44.442	44.688	0.55	44.442	45.025	45.015	16.04
(1,4,1)	8	8	47.810	47.895	0.18	47.810	47.878	47.876	5.33
(2,3,1)	9	9	52.325	52.480	0.30	52.325	52.890	52.875	14.57
(1,1,2)	10	10	60.167	60.146	−0.04	60.170	60.557	60.251	11.30
(2,4,1)	11	11	64.566	64.645	0.12	64.566	65.096	65.075	12.73
(1,5,1)	12	12	66.565	66.708	0.22	66.565	66.634	66.631	4.57
(2,0,2)	13	13	**69.351**	**69.308**	−0.06	**69.351**	**69.351**	69.351	**0.00**
(0,2,2)	14	14	**69.370**	**69.326**	−0.06	**69.383**	**81.266**	71.927	**52.06**
(3,1,1)	15	15	72.953	73.786	1.14	72.953	74.515	74.482	20.37
(3,2,1)	16	16	75.679	76.371	0.91	75.679	77.239	77.197	20.00
(2,5,1)	17	17	80.338	80.360	0.03	80.339	80.830	80.803	11.01
(3,3,1)	18	18	81.256	81.734	0.59	81.256	82.788	82.732	19.14
(2,1,2)	19	19	84.998	84.919	−0.09	85.003	85.653	85.137	12.30
(1,6,1)	20	20	87.064	87.245	0.21	87.064	87.136	87.131	4.05
(3,4,1)	21	21	90.282	90.511	0.25	90.282	91.749	91.678	17.81
(2,6,1)	22	22	98.622	98.578	−0.05	98.623	99.080	99.048	9.60
(1,2,2)	23	23	102.492	102.430	−0.06	102.507	102.554	102.518	3.01
(3,5,1)	24	24	102.690	102.665	−0.02	102.690	104.070	103.984	16.23
(3,0,2)	25	25	**103.966**	**103.821**	−0.14	**103.966**	**103.966**	103.966	**0.00**
(0,3,2)	26	26	**104.029**	**103.881**	−0.14	**104.076**	**121.887**	107.970	**52.05**
(4,1,1)	27	27	106.125	107.518	1.31	106.125	108.916	108.819	22.49
(4,2,1)	*29*	*28*	108.314	109.494	1.09	108.314	111.094	110.982	22.23
(1,7,1)	*28*	*29*	108.727	108.884	0.14	108.727	108.800	108.794	3.67
(4,3,1)	30	30	112.660	113.508	0.75	112.660	115.402	115.269	21.67
(3,1,2)	31	31	114.892	114.690	−0.18	114.900	115.396	115.005	9.27
(3,6,1)	32	32	117.955	117.666	−0.25	117.955	119.239	119.140	14.63
(2,7,1)	33	33	118.628	118.466	−0.14	118.629	119.058	119.021	8.48
(4,4,1)	*35*	*34*	119.704	120.137	0.36	119.704	122.370	122.211	20.76
(2,2,2)	*34*	*35*	119.849	119.680	−0.14	119.868	120.443	119.994	9.76
(4,5,1)	36	36	129.636	129.605	−0.02	129.636	132.190	132.005	19.56
(1,8,1)	37	37	131.195	131.224	0.02	131.195	131.269	131.262	3.36
(3,7,1)	38	38	135.435	134.844	−0.44	135.435	136.628	136.517	13.18
(1,1,3)	*41*	*39*	138.458	138.646	0.14	138.559	145.119	139.827	*29.73*
(4,0,2)	*39*	*40*	**138.510**	**138.163**	−0.25	**138.510**	**138.510**	138.510	**0.00**
(0,4,2)	*40*	*41*	**138.658**	**138.306**	−0.25	**138.769**	**162.495**	144.107	**52.03**
(5,1,1)	*43*	*42*	139.233	141.107	1.35	139.233	143.376	143.165	23.87
(2,8,1)	*42*	*43*	139.830	139.453	−0.27	139.830	140.236	140.195	7.60
(5,2,1)	*46*	*44*	141.101	142.490	0.98	141.101	145.225	144.996	23.66
(4,6,1)	*44*	*45*	142.285	141.756	−0.37	142.286	144.705	144.495	18.21
(3,2,2)	*45*	*46*	142.504	142.158	−0.24	142.535	143.399	142.727	10.96
(1,3,2)	47	47	142.630	142.694	0.05	142.702	145.388	143.409	19.13
(5,3,1)	48	48	144.716	145.865	0.79	144.716	148.795	148.536	23.25
(4,1,2)	49	49	146.781	146.360	−0.29	146.793	147.132	146.868	6.79
(5,4,1)	50	50	150.515	151.095	0.38	150.515	154.513	154.220	22.60

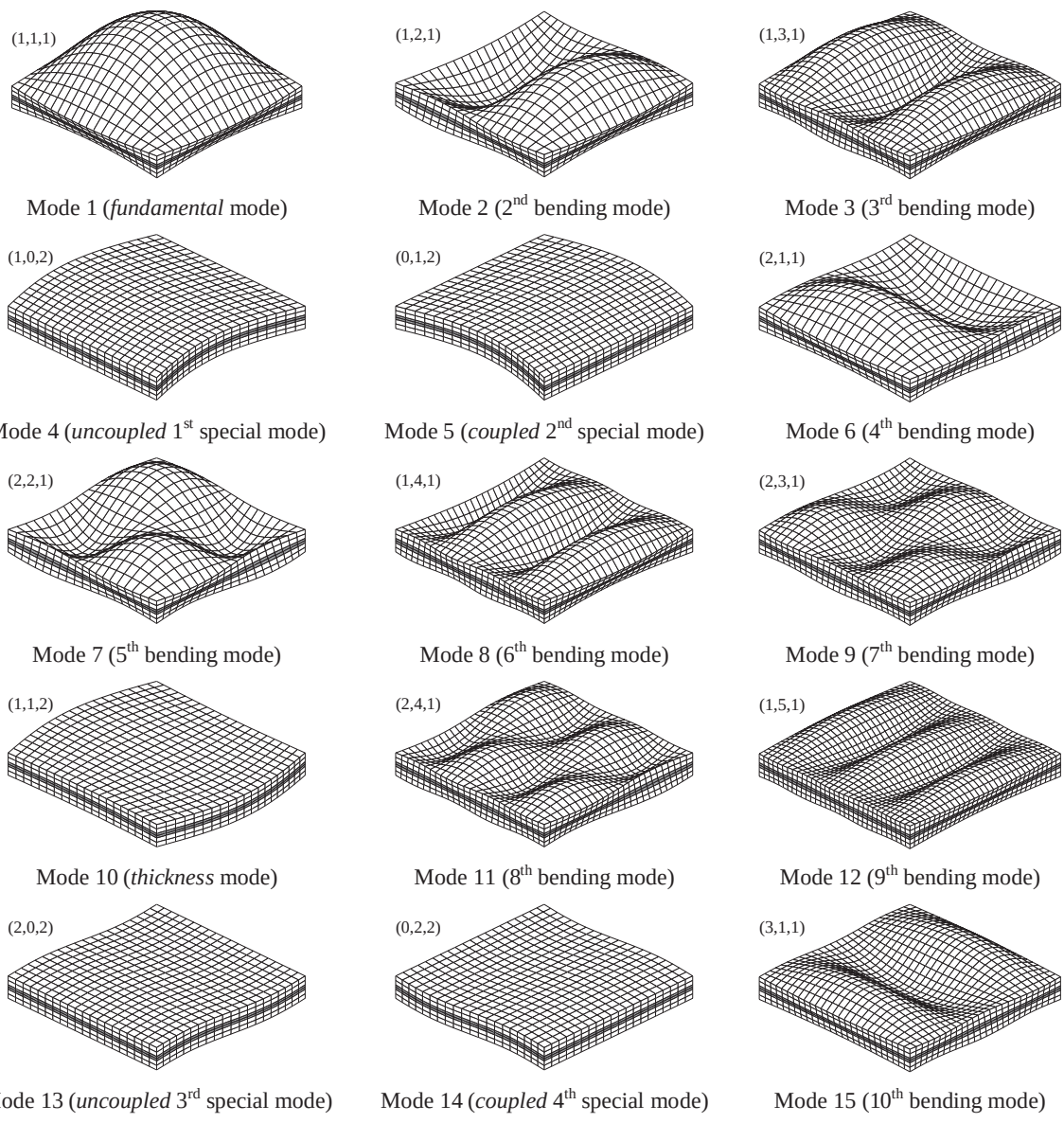

Fig. 4. First 15 modal shapes of a SS adaptive sandwich plate with a SC shear-mode piezoceramic core.

whereas $(0, m_y = 1\text{–}4,\ 2)$ ones are *coupled* and have the highest EMCC ($\sim$52%) independently of the mode order. Notice that the special modes corresponding to $m_z = 1$ can be obtained with the MSSA solution but are not presented here because they were not provided by the 3D FE analysis.

- For the other modes, the effective modal EMCC is higher and increases with m_x (poling direction), but slightly decreases with m_y. The highest EMCC of 29.73 % was obtained for the $(1, 1, 3)$ thickness mode (see later the parametric analysis).

In order to confirm the above expected results regarding the electric state variables thickness distributions, primary and secondary state variables thickness variations are now studied for the fundamental mode

(1,1,1), the first coupled (0,1,2) and uncoupled (1,0,2) special modes and the two thickness modes (1,1,2) and (1,1,3) present in Table 2.

For the fundamental mode, it was found that the EBC have almost no influence on the mechanical and in-plane electric displacements. However, they affect strongly the electric potential and transverse displacement (Fig. 5). As expected, the former are even nil in the conducting elastic faces. This is also true for the SC/OC electric potential and transverse electric displacement, but not for the NE case (Fig. 5). This figure shows also that the electric potential is continuous for the SC interfaces and discontinuous for the OC ones, whereas the transverse electric displacement has the opposite behavior. These results confirm the above expected ones for the conducting elastic faces and the SC/OC interfaces.

Fig. 6 shows the thickness distributions of the *non-nil* mechanical displacements, in-plane electric displacements, and stresses of the special mode (1,0,2) for the different EBC allowed for the shear-mode core. It confirms that the only non-nil displacements are those along the y-axis. As expected, the electric potential and transverse electric displacement were found nil and the only non-nil stresses are the in-plane and y–z transverse shear components (Fig. 6c and d). Besides, the EBC have no influence on any of the non-nil state variables. This is because this special mode is *uncoupled* as mentioned above (EMCC = 0).

Fig. 7 shows the thickness distributions of the *non-nil* mechanical displacements and stresses, and in-plane electric displacements of the special mode (0,1,2) for the different EBC. It confirms that the only non-nil components are the mechanical displacement along the x-axis (poling direction) and the electric displacement along the perpendicular direction (y-axis). In contrary to the previous mode, the non-nil mechanical displacement and stresses distributions are influenced by the EBC. This is due to the fact that this mode is *highly coupled* (EMCC = ~52%) as can be seen also from Fig. 8 which shows non-nil electric potential and transverse electric displacement.

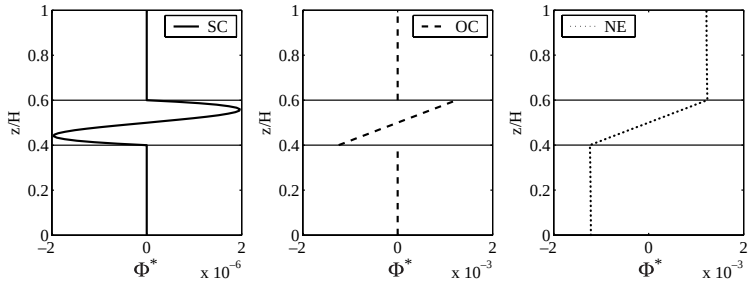

(a) Electric potential

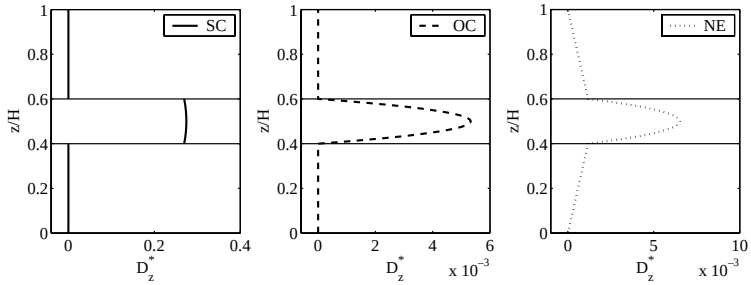

(b) Transverse electric displacement

Fig. 5. Thickness distributions of electric potential and transverse electric displacement for the fundamental mode (1,1,1) of a SS shear-mode adaptive sandwich plate with different electric boundary conditions.

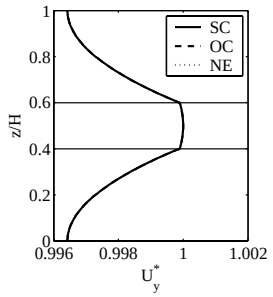

(a) 1st special mode mechanical y-displacement

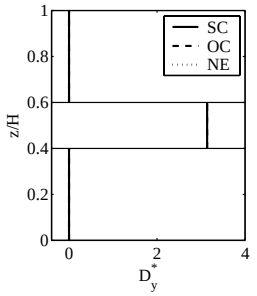

(b) 1st special mode electric y-displacement

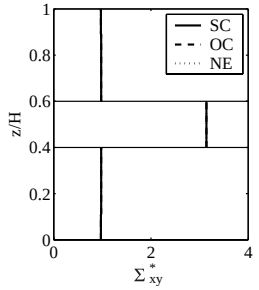

(c) 1st special mode in-plane shear stress

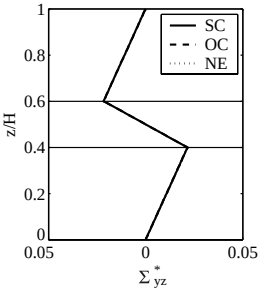

(d) 1st special mode transverse shear yz-stress

Fig. 6. Thickness distributions of *non-nil* electromechanical state variables for the special mode $(1,0,2)$ of a SS shear-mode adaptive sandwich plate with different electric boundary conditions.

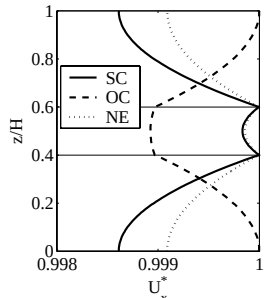

(a) 2nd special mode mechanical x-displacement

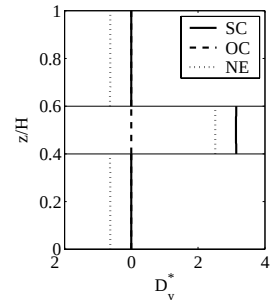

(b) 2nd special mode electric y-displacement

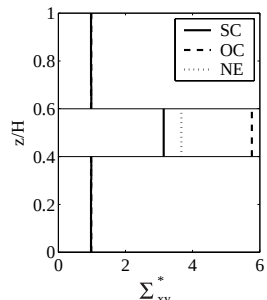

(c) 2nd special mode in-plane shear stress

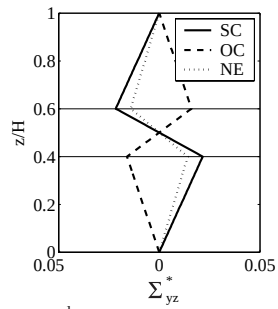

(d) 2nd special mode transverse shear xz-stress

Fig. 7. Thickness distributions of *non-nil* mechanical and in-plane electric state variables for the special mode $(0,1,2)$ of a SS shear-mode adaptive sandwich plate with different electric boundary conditions.

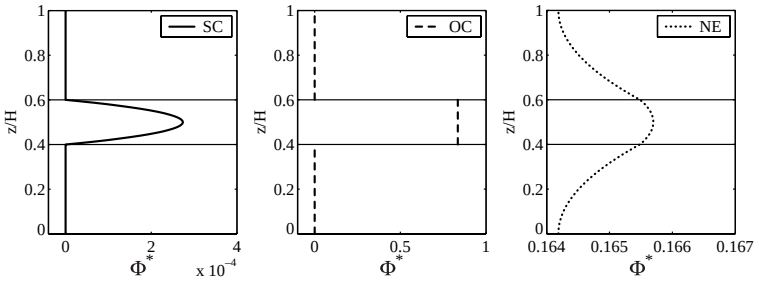

(a) Electric potential

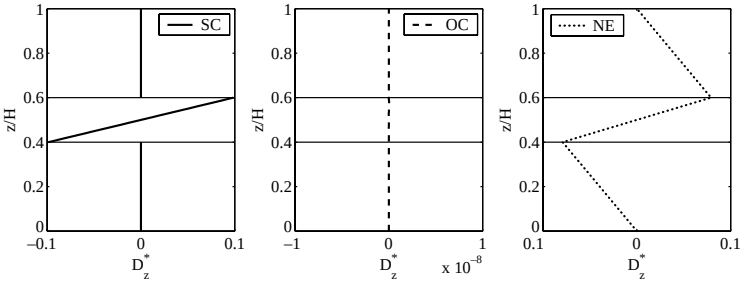

(b) Transverse electric displacement

Fig. 8. Thickness distributions of electric potential and transverse electric displacement for the special mode $(0,1,2)$ of a SS shear-mode adaptive sandwich plate with different electric boundary conditions.

The thickness distributions of the mechanical and in-plane electric displacements of the first thickness mode $(1,1,2)$ of the SS adaptive plate are shown in Fig. 9 for the different EBC. This mode is a membrane one, dominated by the y-displacement. The electric potential and transverse electric displacement are also strongly affected by the EBC (Fig. 10). As expected, the latter are nil in the elastic faces for SC and OC electroded core. Notice the exchange of profiles between the electric potential and transverse electric displacement for the SC and OC EBC. Besides, in contrary to the fundamental $(1,1,1)$ and special $(0,1,2)$ modes, NE profiles do not follow either SC or OC ones.

The stress distributions of the mode $(1,1,2)$ are shown in Fig. 11. The latter indicates that the in-plane stresses are layer-wise constant and dominant, confirming the mode membrane behavior. Here, the EBC affect almost all stresses. Notice that the transverse shear stresses are piecewise linear, while the transverse normal one is piecewise nonlinear.

The *most coupled* thickness mode $(1,1,3)$ is also a membrane one, but dominated by the displacement in the poling direction and presents a small transverse shear behavior. The EBC affect its in-plane displacements, almost as in Fig. 10, and the electric transverse displacement and potential, as in Fig. 12. In contrary to the fundamental mode $(1,1,1)$, here the distributions of the latter are similar for NE and SC core. For the OC case, the electric potential is constant; whereas, the transverse electric displacement is almost nil.

The analysis of the stress distributions of the mode $(1,1,3)$ indicates that the in-plane stresses are, as in Fig. 11, nearly layer-wise constant and dominant, confirming the mode dominant membrane behavior. Here also, the EBC affect all stresses in the core. Their transverse components are piecewise linear except for the transverse normal one.

In summary, the results presented in this sub-section have confirmed all expected theoretical results predicted in the previous sub-sections regarding the distributions and interfaces continuities of the electric state variables as well as those concerning the special modes corresponding to $m_x = 0$ or $m_y = 0$. This validates then the proposed MSSA solution.

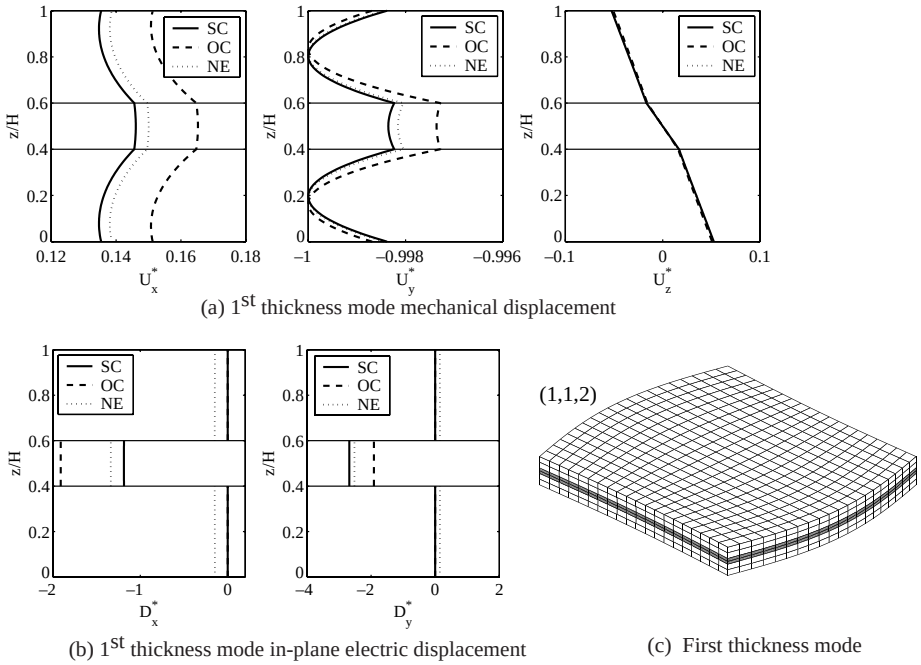

(a) 1st thickness mode mechanical displacement

(b) 1st thickness mode in-plane electric displacement

(c) First thickness mode

Fig. 9. Thickness distributions of mechanical and in-plane electric displacements for the thickness mode (1, 1, 2) of a SS shear-mode adaptive sandwich plate with different electric boundary conditions.

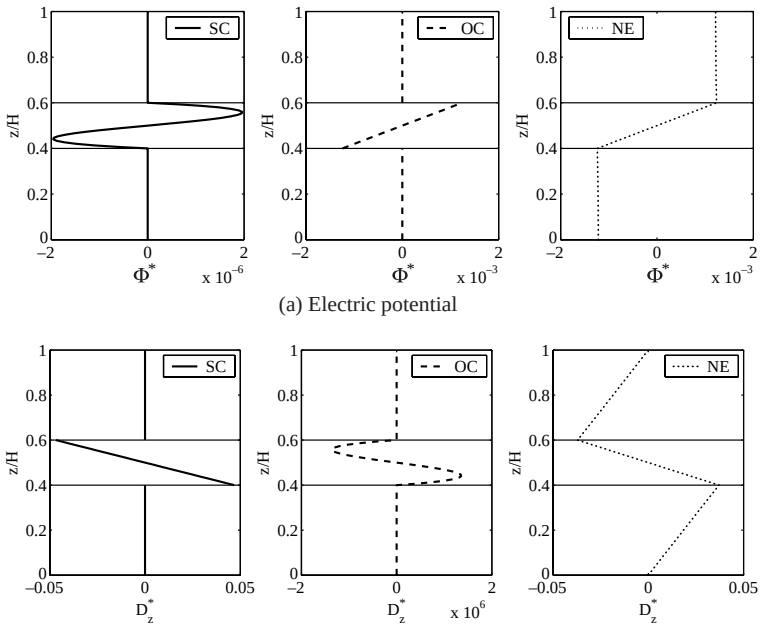

(a) Electric potential

(b) Transverse electric displacement

Fig. 10. Thickness distributions of electric potential and transverse electric displacement for the thickness mode (1, 1, 2) of a SS shear-mode adaptive sandwich plate with different electric boundary conditions.

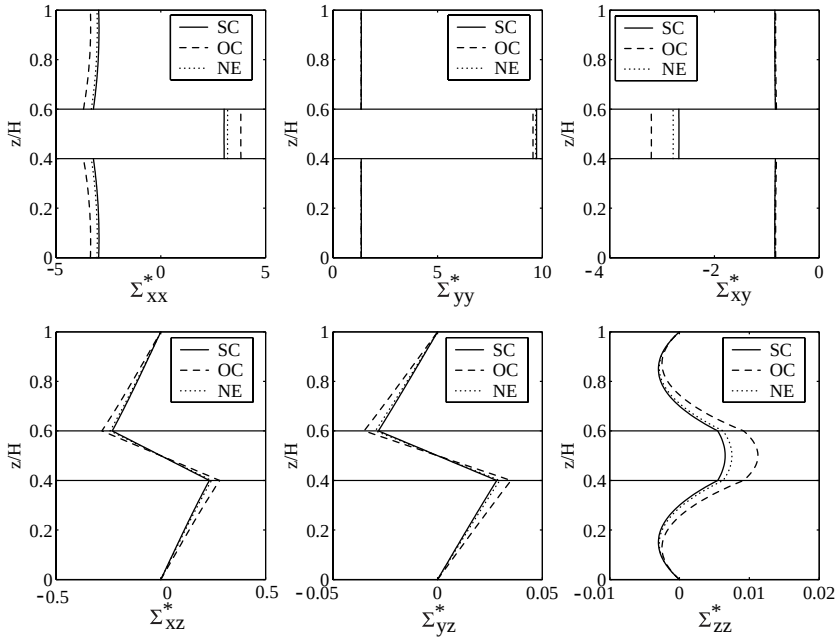

Fig. 11. Thickness distributions of the stresses for the thickness mode (1, 1, 2) of a SS shear-mode adaptive sandwich plate with different electric boundary conditions.

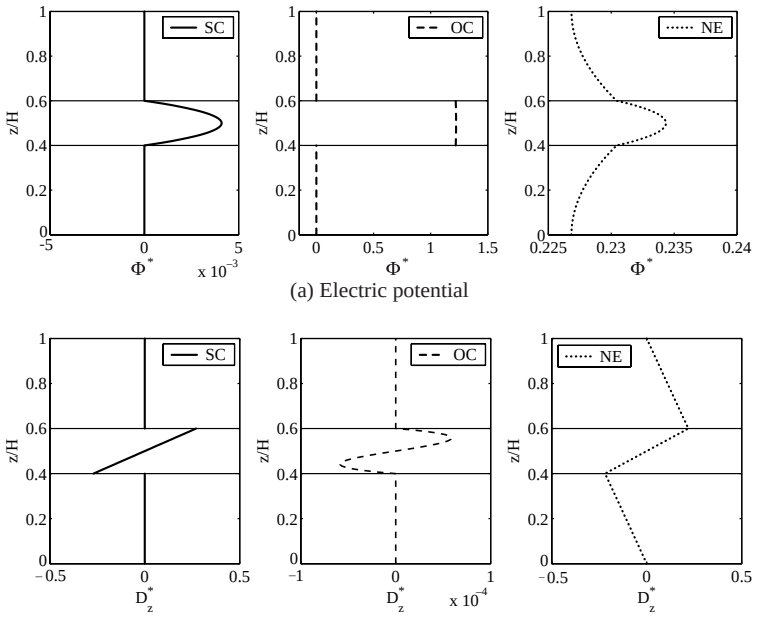

Fig. 12. Thickness distributions of electric potential and transverse electric displacement for the thickness mode (1, 1, 3) of a SS shear-mode adaptive sandwich plate with different electric boundary conditions.

7. Parametric analysis

Since the MSSA has been validated, focus is now made on the parametric analysis of the effective modal EMCC of in-plane $(m_x, m_y, 1)$ and thickness $(1, 1, m_z)$ modes with regard to variations of the EBC, plate side-to-thickness ratio (L/H), shear-mode piezoceramic core-to-plate thickness ratio (H_{PZT}/H) and the shear-mode piezoceramic lamina thickness position in a laminated plate. Unless otherwise indicated, the basic configuration is that used in the previous validation section; i.e., the relatively thick ($L/H = 10$, $H = 1$cm) SS square sandwich plate with $0.4H$-thick 0°-GE composite elastic faces and $0.2H$-thick PZT-5H piezoceramic core. The material properties are also those of Table 1.

7.1. In-plane $(m_x, m_y, 1)$ modes

In-plane modes are the most studied in the reference solutions. They are also the easiest to get with finite elements. Since, the latter use generally only the electric potential as electric degree of freedom, only SC EBC can be imposed properly. As seen in the previous section (see Table 2), the SC natural frequencies differ only slightly from the elastic ones. It is then natural to start this parametric analysis by studying the relative difference between SC and EL circular frequencies for different in-plane modes.

As expected, Fig. 13 indicates that the relative differences between SC and EL circular frequencies increases with increasing the (m_x, m_y) mode order and decreasing the plate side-to-thickness ratio but remains very small (less than 0.01 % for the thick plate and $m_x = m_y = 10$ case (Fig. 13b)). For the most studied mode $(1, 1, 1)$, this relative difference does not exceed 0.03 % even for a thick plate ($L/H = 5$) with the piezoceramic core constituting 90% of the total thickness (Fig. 13c). It is then concluded, that SC EBC are not sufficient to validate piezoelectric finite elements but OC ones should be considered also. With the latter the difference is greater and both SC and OC EBC are useful for the evaluation of the effective modal EMCC as made in the previous section and hereafter.

Although quasi exclusively considered in the literature, perfect electric bonding interfaces, which are equivalent to NE EBC as shown in the previous section, are in fact useless in practice for both extension- and shear-mode inner piezoceramic laminae. To be used as actuators or sensors, embedded piezoelectric layers have to be electroded. The possible EBC are then either SC or OC. Natural frequencies under the latter EBC can be exploited to evaluate the effective modal EMCC as defined previously by Eq. (70).

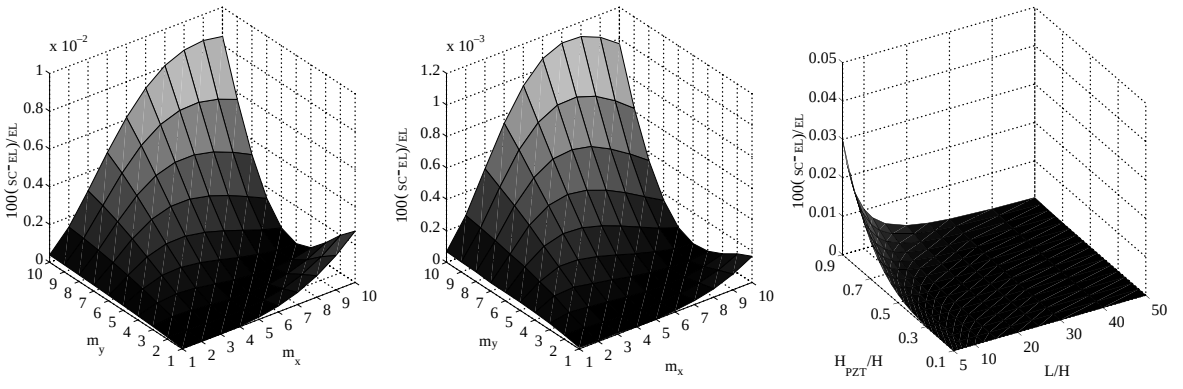

(a) L/H=5 (b) L/H=10 (c) *Fundamental mode (1,1,1)*

Fig. 13. Variation of the relative difference between SC and EL circular frequencies with m_x, m_y, L/H and H_{PZT}/H of a SS shear-mode adaptive sandwich plate.

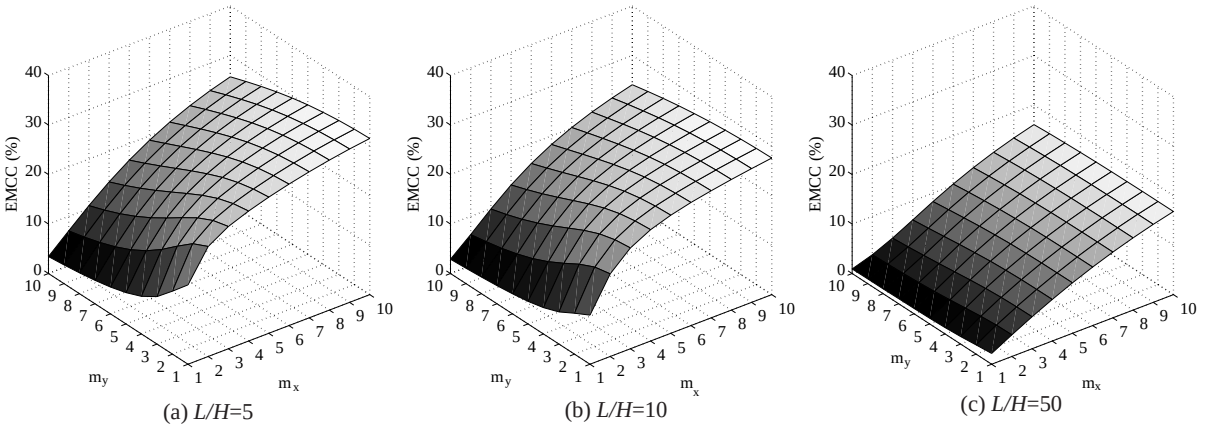

Fig. 14. Variation of the EMCC with m_x and m_y for different thickness ratios L/H of a SS shear-mode adaptive sandwich plate.

Fig. 14 indicates that the effective modal EMCC increases with increasing m_x but decreases slightly with increasing m_y mode order. Besides, it augments much more rapidly and with higher values than the relative difference between SC and EL natural frequencies (Fig. 13). The EMCC increases also with decreasing the plate side-to-thickness ratio and, as expected for the shear-mode piezoceramic materials, is higher for thick plates (Fig. 14a).

7.2. Thickness $(1,1,m_z)$ modes

Most of the reference solutions available in the open literature have focused mainly on the previous in-plane modes. Thus, the so-called thickness modes corresponding to $m_x = m_y = 1$ are generally less studied, except the fundamental mode, because they are considered very high in the modes order of appearance. As can be seen from Table 2, this is not true in the sense that the thickness mode $(1,1,2)$ is the 10th one whereas the thickness mode $(1,1,3)$ is the 39th one. Besides, in the analyzed example, the latter is even the most coupled mode after the special modes $(0,m_y,2)$. So, both thickness modes are to be considered when constructing a modal basis using the first 40 modes for example. It is then the objective of this sub-section to present the same parametric analysis as that conducted for the in-plane modes. Additionally, here the influence of the position of the shear-mode piezoceramic core through-the-thickness of a SS laminated plate is also studied.

Fig. 15 shows the effective modal EMCC variations with the plate side-to-thickness ratio, L/H, and the core-to-plate thickness ratio, H_{PZT}/H for the first three thickness modes $(1,1,m_z = 1-3)$. Hence, Fig. 15a indicates that, for the fundamental (bending) mode, the EMCC is optimum for a thick plate with the piezoceramic core occupying almost 50%. However, this configuration is minimal for the 2nd (membrane) mode. The most coupled mode (3rd) tends to reach, for $L/H = 10$, $H_{PZT}/H = 0.9$, the PZT-5H material EMCC of 70%.

To analyze the effect of the variation of the thickness position of the shear-mode piezoceramic lamina on the effective modal EMCC, a PZT-5H lamina of thickness $0.2H$ is moved through the thickness of an 8-layer composite plate according to the 7 positions shown in Table 3. Each lamina is made of 0°-GE and has a thickness of $0.1H$, so that the layered plate keeps its total thickness of $H = 1$cm and its side-to-thickness ratio $L/H = 10$.

The results presented in Fig. 16 for the first three thickness modes indicates that the fundamental mode presents a minimum EMCC for the 4th position, whereas for the other two thickness modes the EMCC is

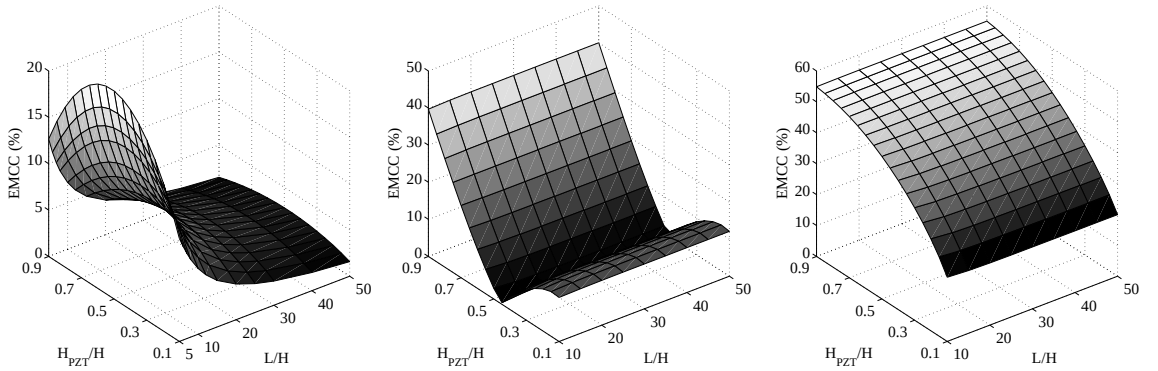

(a) Mode (1,1,1) (b) Mode (1,1,2) (c) Mode (1,1,3)

Fig. 15. Variation of the EMCC with L/H and H_{PZT}/H for a SS shear-mode adaptive sandwich plate.

Table 3
Positions of the shear-mode piezoceramic lamina in the SS laminated plate

Position	Lamination sequence
1	$(0°\text{-GE})_1$ /PZT-5H/$(0°\text{-GE})_7$
2	$(0°\text{-GE})_2$ /PZT-5H/$(0°\text{-GE})_6$
3	$(0°\text{-GE})_3$ /PZT-5H/$(0°\text{-GE})_5$
4	$(0°\text{-GE})_4$ /PZT-5H/$(0°\text{-GE})_4$
5	$(0°\text{-GE})_5$ /PZT-5H/$(0°\text{-GE})_3$
6	$(0°\text{-GE})_6$ /PZT-5H/$(0°\text{-GE})_2$
7	$(0°\text{-GE})_7$ /PZT-5H/$(0°\text{-GE})_1$

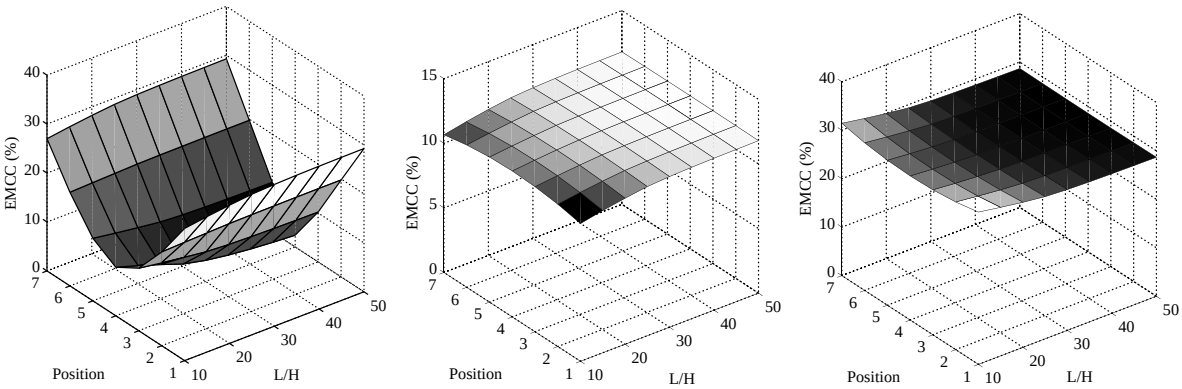

(a) Mode (1,1,1) (b) Mode (1,1,2) (c) Mode (1,1,3)

Fig. 16. Variation of the EMCC with L/H and the shear-mode core position in a SS adaptive laminated plate.

nearly insensitive to the position and side-to-thickness ratio parameters. This can be explained by the fact that the last two modes have a dominant membrane behavior whereas, the fundamental mode is a bending one.

8. Summary and conclusions

An exact 3D mixed state space solution has been presented for the free-vibration of multilayer composite SS plates with inner NE or SC/OC electroded *shear mode* piezoceramic layers. It has the major advantage that the resulting eigenvalue problem is only of order 3 or 4, depending on the presence or not of inner electrodes, independently of the number of layers constituting the laminate. For NE interfaces, full electromechanical continuity conditions are satisfied; whereas for electroded (OC or SC) interfaces, the physical discontinuity of the dual state variable to the known (prescribed) one is handled via analytical condensations of the electric state variables at the laminae transfer matrices level; i.e., prior to the laminate assembly. After discussing its implementation and computational aspects, the proposed exact solution has been validated via some demonstrated expected theoretical results concerning the behavior of a SS adaptive sandwich plate with conducting elastic faces and a shear-mode piezoceramic core. In particular, it was demonstrated and confirmed by the numerical analysis that:

- For the considered SC and OC configurations, the electric state variables are *nil* in the conducting elastic faces. However, for the NE configuration, the popular electric perfect bonding assumption at the interfaces make these variables non-nil inside the conducting elastic faces;
- The electric transverse displacement and potential are *discontinuous* at an electroded interface when the dual electric state variable is known. Thus, the widespread electric perfect bonding assumption (continuous electric transverse displacement and potential) is meaningless for an embedded electroded piezoceramic lamina;
- In contrary to the extension-mode piezoceramic materials, the use of the shear-mode ones in a SS adaptive sandwich plate leads to *coupled* $(0, m_y)$ and uncoupled $(m_x, 0)$ special modes often missed by the available exact solutions. The coupled modes provide even the highest EMCC ($\sim 52\%$) almost independently of m_y. However, they have only theoretical importance and their practical usefulness is still to be proved.

After its validation, the MSSA has been used for a parametric analysis of the EMCC of in-plane and thickness modes through variations of the plate length-to-thickness ratio, the shear mode piezoceramic thickness and its position through-the-thickness of a laminated plate. It was found that:

- The relative differences between SC and EL frequencies increase with increasing the (m_x, m_y) mode order and with decreasing the plate side-to-thickness ratio but remains very small. For example, it does not exceed 0.03% for the fundamental mode even for a thick plate ($L/H = 5$) with a piezoceramic core of 90% of the total thickness;
- The effective modal EMCC increases with increasing m_x but decreases slightly with increasing m_y mode order much more rapidly and with higher values than the relative difference between SC and EL natural frequencies. It increases also with decreasing the plate side-to-thickness ratio and, as expected for the shear-mode piezoceramic materials, it is higher for thick plates;
- For the fundamental (bending) mode, the EMCC is optimum for a thick plate with the piezoceramic core occupying almost 50%. However, this configuration is minimal for the 2nd (membrane) thickness mode. The most coupled mode (3rd thickness mode) tends to reach, for $L/H = 10$ and $H_{\mathrm{PZT}}/H = 0.9$, the PZT-5H material EMCC of 70%;
- The fundamental mode presents a minimum EMCC for the mid-laminate thickness position of the shear-mode piezoceramic core whereas, for the other two thickness modes, the EMCC is nearly insensitive to the shear-mode piezoceramic core thickness position and plate side-to-thickness ratio parameters.

- The above results can serve for *physical understanding* of the transverse shear-mode piezoelectric materials behavior. The latter are used, for example, for active vibration control and passive shunted damping. These exact results can also be used by design engineers or researchers for validation of approximate analytical/numerical 2D solutions.

References

Bahar, L.Y., 1977. A mixed method in elasticity. Journal of Applied Mechanics 44, 790–791.

Batra, R.C., Aimmanee, S., 2003. Missing frequencies in previous exact solutions of free vibrations of simply supported rectangular plates. Journal of Sound and Vibration 265, 887–896.

Batra, R.C., Liang, X.Q., 1997. The vibration of a rectangular laminated elastic plate with embedded piezoelectric sensors and actuators. Computers and Structures 63 (2), 203–216.

Benjeddou, A., 2000. Advances in piezoelectric finite element modeling of adaptive structural elements: a survey. Computers and Structures 76 (1–3), 347–363.

Benjeddou, A., Deü, J.-F., 2001a. Piezoelectric transverse shear actuation and sensing of plates—part 1: a three-dimensional mixed state space formulation. Journal of Intelligent Material Systems and Structures 12, 435–449.

Benjeddou, A., Deü, J.-F., 2001b. Piezoelectric transverse shear actuation and sensing of plates - part 2: application and analysis. Journal of Intelligent Material Systems and Structures 12, 450–467.

Benjeddou, A., Deü, J.-F., 2002. A two-dimensional closed-form solution for the free-vibrations analysis of piezoelectric sandwich plates. International Journal of Solids and Structures 39, 1463–1486.

Benjeddou, A., Deü, J.-F., Letombe, S., 2002. Free-vibrations of simply-supported piezoelectric adaptive plates: an exact sandwich formulation. Thin-Walled Structures 40, 573–593.

Benjeddou, A., Deü, J.-F., 2003. Parametric free-vibration analysis of laminated plates with embedded shear-mode piezoceramic layers. In: The Mini-Symposium on "Theoretical, Modeling and Simulation Aspects of Smart Materials and Structures", during the 6th Hellenic European Research for Computer Mathematics and its Applications, Athens, Greece, September 25–27, 2003.

Chen, W.Q., Xu, R.Q., Ding, H.J., 1998. On free vibration of piezoelectric composite rectangular plate. Journal of Sound and Vibration 218 (4), 741–748.

Deü, J.-F., Benjeddou, A., 2002. Exact free-vibrations analysis of laminated plates with embedded piezoelectric transverse shear actuators and sensors. In: Mang, H.A., Rammerstorfer, F.G., Eberhardsteiner, J. (Eds.), CD-ROM Proceedings of the Fifth World Congress on Computational Mechanics. WCCMV, Vienna, Austria.

Ding, H.J., Chen, W.Q., Xu, R.Q., 2000. New state space formulations for transversely isotropic piezoelectricity with applications. Mechanics Research Communications 27 (3), 319–326.

Heyliger, P., Saravanos, D.A., 1995. Exact free-vibration analysis of laminated plates with embedded piezoelectric layers. Journal of the Acoustical Society of America 98 (3), 1547–1557.

Lee, J.S., Jiang, L.Z., 1996. Exact electroelastic analysis of piezoelectric laminae via state space approach. International Journal of Solids and Structures 33 (7), 977–990.

Liang, X.Q., Batra, R.C., 1997. Changes in frequencies of a laminated plate caused by embedded piezoelectric layers. AIAA Journal 35 (10), 1672–1673.

Rogacheva, N.N., 1994. The Theory of Piezoelectric Shells and Plates. CRC Press, Boca Raton.

Saravanos, D.A., Heyliger, P.R., 1999. Mechanics and computational models for laminated piezoelectric beams, plates and shells. Applied Mechanics Reviews 52 (10), 305–320.

Tarn, J.Q., 2002. A state space formalism for piezothermoelasticity. International Journal of Solids and Structures 39, 5173–5184.

Tarn, J.Q., Huang, L.J., 2002. Saint-Venant end effects in multilayered piezoelectric laminates. International Journal of Solids and Structures 39, 4979–4998.

Vel, S.S., Batra, R.C., 2001a. Exact solution for the cylindrical bending of laminated plates with embedded shear actuators. Smart Materials and Structures 10, 240–251.

Vel, S.S., Batra, R.C., 2001b. Exact solution for rectangular sandwich plates with embedded piezoelectric shear actuators. AIAA Journal 39, 1363–1373.

Wang, J., Chen, L., Fang, S., 2003. State vector approach to analysis of multilayered magneto-electro-elastic plates. International Journal of Solids and Structures 40, 1669–1680.

Wang, J., Fang, S., Chen, L., 2002. The state vector methods for space axisymmetric problems in multilayered piezoelectric media. International Journal of Solids and Structures 39, 3959–3970.

Xu, K., Noor, A.K., Tang, Y.Y., 1997. Three-dimensional solutions for free-vibrations of initially stressed thermo-electromechanical multilayered plates. Computer Methods in Applied Mechanics and Engineering 141, 125–139.

Zhang, C., Cheung, Y.K., Di, S., Zhang, N., 2002. The exact solution of coupled thermoelectroelastic behavior of piezoelectric laminates. Computers and Structures 80, 1201–1212.

Zhang, X.D., Sun, C.T., 1999. Analysis of a sandwich plate containing a piezoelectric core. Smart Materials and Structures 8, 31–40.

Zhong, Z., Shang, E.T., 2003. Three-dimensional exact analysis of a simply supported functionally gradient piezoelectric plate. International Journal of Solids and Structures 40, 5335–5352.